PREDICTING FRACTURE DENSITY IN THE EAGLE FORD (BOQUILLAS) FORMATION, VAL VERDE BASIN, TEXAS

by

SEAN KIMIAGAR

Presented to the Faculty of the Graduate School of
The University of Texas at Arlington in Partial Fulfillment
of the Requirements
for the Degree of

MASTER OF SCIENCE IN GEOLOGY

THE UNIVERSITY OF TEXAS AT ARLINGTON
December 2013

ACKNOWLEDGEMENTS

I would like to take this opportunity to thank those who supported me throughout the project and the master's degree as a whole. I would like to thank University of Texas at Arlington and the Department Earth and Environmental Sciences for the material and technical support, through access to academic material and highly-regarded professors; Dr. John Wickham for his time, knowledge, guidance and mentorship throughout the two years at UTA and specially throughout the thesis process; Dr. Larry Standlee and Dr. Qinhong Hu for their time and guidance; and Dr. Xinbao Yu for his time as well as providing access to the Civil Engineering Geomechanics Lab and its helpful staff. I would also like to thank my family and friends for their support and understanding throughout the two years.

July 22, 2013

ABSTRACT

PREDICTING FRACTURE DENSITY IN THE
EAGLE FORD (BOQUILLAS) FORMATION,
VAL VERDE BASIN, TEXAS

Sean Kimiagar, M.S.

The University of Texas at Arlington, 2013

Supervising Professor: John Wickham

Fracture density in hydrocarbon reservoirs is an important variable for efficient production of oil and gas in tight reservoirs. Fracture density is the fracture surface area per unit of volume, and the higher the reservoir fracture density, the higher its recovery factor. Being able to estimate the induced fracture density in advance of hydraulic fracturing will therefore help increase the knowledge of the reservoir and production efficiency. Theoretical considerations indicate that fracture density is related to strain energy. The purpose of this study is to verify the hypothesis that fracture density can be predicted under constant strain conditions using the elastic properties, rock density and fracture toughness. The hypothesis has been framed in the form of an equation, the validity of which is to be tested. In order to do so, a number of field and laboratory measurements were made. In the field, the fracture densities of outcrops were measured and samples collected. In the laboratory, density and elastic properties of the rocks were measured using ultrasonic techniques. In order to maintain the assumption that the strain in the strata where measurements are made remains constant, samples are

taken from different sedimentary layers in the same outcrop, as well as fracture measurements from the same joint set. The hypothesis was not confirmed. Two of the possibilities for the outcome could be either the samples' spatial distribution, with the samples being either from the same outcrop or outcrops in excess of 20 miles apart, or the assumption of constant strain throughout the samples, which may not be valid in the sample area.

TABLE OF CONTENTS

LIST OF ILLUSTRATIONS

Figure Page

LIST OF TABLES

CHAPTER 1

INTRODUCTION

Over the years considerable work has been done on the relationship between strain energy and fracturing. The relationship between strain energy and fracture density however, has not been extensively investigated. Over the past decades, numerous studies have been conducted on fracture density and fracture spacing (Narr and Lerche, 1984; Watts, 1983; Willemse et al., 1997; Julander et al., 1999; Tappet al., 1999; Maulden, Dunne and Rohrbaught, 2001; Di Naccio et al., 2005; Ortega, Marrett and Laubach, 2006; Lorenz Cooper and Olsson, 2006; Mclennan et al., 2009; Zahm and Hennings, 2009; Barthelemy, Guiton and Daniel, 2009, among others). Recently, seismic methods have been used to characterize subsurface fractures from P-wave velocity reduction (Karaman et al., 1997), shear-wave splitting (Lou and Rial, 1997), frequency-dependent anisotropy (Maultzsch et. al., 2003), Azimuthal AVO analysis (Xu and Tsvankin, 2007) and monitoring the artificial fracturing process in real time (Maxwell and Urbancic, 2005).

Fracture spacing and density are affected by a number of factors. Some of these factors are layer curvature (Murray, 1968; Stearns and Friedman, 1972; Schultz-Eia and Yeh,1992), strain magnitude (Hennings, Olson and Thompson, 2000), elastic stress (Bourne and Willemse, 2001), layer thickness and stress shadows (Ladeira and Price, 1981; Huang and Angelier, 1989; Pollard and Segal, 1987), porosity (Lezin et al., 2009), Young's Modulus (Palchik and Hatzor, 2002) and rock strength (Corbett et al., 1987)*.

* Much of the introduction has been taken from Wickham & Yu 2012.

Most of the work on the factors controlling fracture density has been done empirically. As a result, the data has been handled as if it were produced by a stochastic process. Three recent examples exist: One that uses regression, one that uses Bayesian statistics and one that uses artificial neural networks and probabilistic logic.

This research tests a geomechanical hypothesis, relating strain energy to fracture density. The hypothesis makes a number of simplifying assumptions, therefore verifying it is important. If the simplified hypothesis is adequate, acoustic and density logs can be used to estimate the fracture density potential of stratigraphic layers in the subsurface before designing a hydraulic fracturing operation. The data used in this study were collected through three methods: (1) Fracture density measurements made on various stratigraphic layers in the field, (2) density measurements on rock samples collected from those layers, and (3) acoustic velocity measurements on those same samples made in the Geomechanics Laboratory of the Civil Engineering Department.

CHAPTER 2

THEORY AND HYPOTHESIS

Table 1 Symbols used throughout the thesis.

Symbol	Meaning
U	Energy
U_v	Strain energy in volume v
V	Volume
A	Area
G	Energy release rate
σ	Stress
ε	Strain
F_d	Fracture Density
U_a	Energy per fracture area created
μ	Elastic Shear Modulus
E	Young's Modulus
v	Poisson's Ratio
V_p	Compressional Wave Velocity
V_s	Shear Wave Velocity
I_1	First Strain Invariant
I_2	Second Strain Invariant
K_{IC}. K_{IIC}, K_{IIIC}	Critical Stress Intensity Factors for Mode I, II, and III

In this study, we hypothesize that Equation 1 (Wickham & Yu, 2012) can be verified, using field and lab data.

Equation 1 Calculating Fracture Density (F_d)

$$\frac{F_d U_a}{\mu} = A\frac{v}{1-2v} + B$$

Symbols represented in Equation 1 are the following: μ represents Elastic Shear Modulus, *v* represents Poisson's Ratio, U_a is a material property,

representing energy per fracture area created. A and B are strain-related constants, which are defined as follows:

Equation 2 Strain-related constant A

$$A = I_1^2$$

Equation 3 Strain-related constant B

$$B = I_1^2 - 2I_2$$

where I_1 is the First Strain Invariant and I_2 the Second Strain Invariant.

In Equation 1 F_d stands for measured fracture density. That is the fracture density value measured in the field. This equation has the form of a straight line *y* = *mx* + *b*. The predicted fracture density can be calculated using a relationship between the shear modulus and Poisson's Ratio and the density of the rocks and the P- and S-wave velocities through the rock sample (See equations 5 and 9). The two sides are then plotted against one-another in order to examine the relationship between the two. A perfect straight line will indicate 100% correlation and accuracy between measured and predicted fracture density, and therefore fully supporting the equation and hypothesis of this research. Given the potential errors in measurements, both in the field and in the lab, 100% correlation is unlikely, but a nearly linear relationship supports the hypothesis to varying degrees as well.

Equation 4 Equation 1 put into words

$$\frac{(Fracture\ Density)\ X\ (Energy\ Per\ Fracture\ Area\ Created)}{Elastic\ Shear\ Modulus} = A\frac{Poisson's\ Ratio}{1-(2\ X\ Poisson's\ Ratio)} + B$$

Equations 5-9 demonstrate how the material properties of Equation 1 can be measured using density, and acoustic velocities. Equation 5 calculates Elastic Shear Modulus, using S-wave velocity and rock density.

Equation 5 Elastic Shear Modulus (Source: Wickham & Yu 2012)

$$\mu = v_s^2 \, X \, \rho$$

Equation 6 calculates the Energy Per Fracture Area, using Critical Energy Release Rate values, calculated using Equation 7.

Equation 6 Energy Per Fracture Area Created (Source: Wickham & Yu 2012)

$$U_a = \frac{G_c}{2}$$

Equation 7 calculates Critical Energy Release Rate, using Young's Modulus and Critical Stress Intensity Factor for Mode I, lithology-dependent fractures, found in literature.

Equation 7 Critical Energy Release Rate (Source: Wickham & Yu 2012)

$$G_c = \frac{K_I^2{}_c}{E}$$

Equation 8 is used to calculate Young's Modulus, using rock density and Poisson's Ratio.

Equation 8 Young's Modulus (Source: Wickham & Yu 2012)

$$E = Young'sModulus = 2 \times \rho \times v_S^2 \times (\sigma - 1)$$

Equation 9 is used to calculate Poisson's Ratio, using P- and S-wave velocities from laboratory-conducted acoustic tests.

Equation 9 Poisson's Ratio (Source: Wickham & Yu 2012)

$$\sigma = \nu = \left[\frac{\left(\frac{1}{2}\right)(v_P^2 - 2v_S^2)}{(v_P^2 - v_S^2)}\right]$$

In this study we have used outcrops to measure fracture density in different stratigraphic layers to use in Equation 1. Samples were collected from those same layers in order to measure the material properties of equation 1. If those layers have been subjected to the same amount of strain, then the data should plot as a straight line using equation 1 with A as the slope and B the intercept.

In the petroleum industry, the material properties can be measured using logging tools. The fracture Toughness, Kic, would have to be measured or estimated from those material properties. Verifying Equation 1 will allow for the prediction of fracture density using a suite of well logs.

CHAPTER 3

GEOLOGIC SETTING

The Upper Cretaceous Eagle Ford Formation, locally called the Boquillas Formation (Figure 1), is well exposed in several deep road cuts along U.S. Highway 90 in Val Verde County, South West Texas (Figure 2). Interest in these outcrops derives from the current Eagle Ford oil and gas play in McMullen, LaSalle, and Maverick counties in the South Texas Maverick Basin, with production from shales and mudrocks (Figure 3). Outcrops in Val Verde County provide an accessible window for improved understanding of the play. The formation is approximately 200 ft thick in Val Verde County, significantly thicker in the producing counties to the East, and over ten times thicker in northern Mexico. The Eagle Ford Formation was deposited during the Cenomanian-Turonian Oceanic Anoxic Event.

Figure 1 shows the Eagle Ford Formation in chronological order, with respect to its neighboring formations. In certain locations along the outcrops, parts of the Atco Chalk and Buda Formations could also be observed. The Eagle Ford Formation was deposited in a water depth of approximately 330 ft, in an area expanding between 12 and 30 miles offshore (Railroad Commission of Texas, www.rrc.state.tx.us/eagleford).

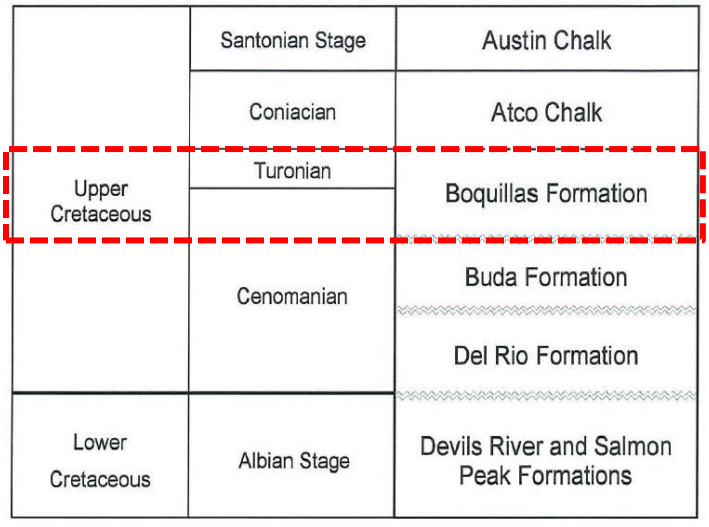

Figure 1 Eagle Ford (Boquillas) Formation geologic age (Source: Lock et al. 2010)

Figure 2 shows the location of the outcrops of interest along Highway 90. The guidebook titled “Eagle Ford (Boquillas) Formation and Associated Strata in Val Verde County, Texas” (Lock et al. 2010) was used in locating the outcrops. The city of Del Rio, circled in red, is approximately 30 miles away from the first outcrop location, and was used as the overnight base while collecting data and samples. The outcrops provide an accessible window for improved understanding of the play.

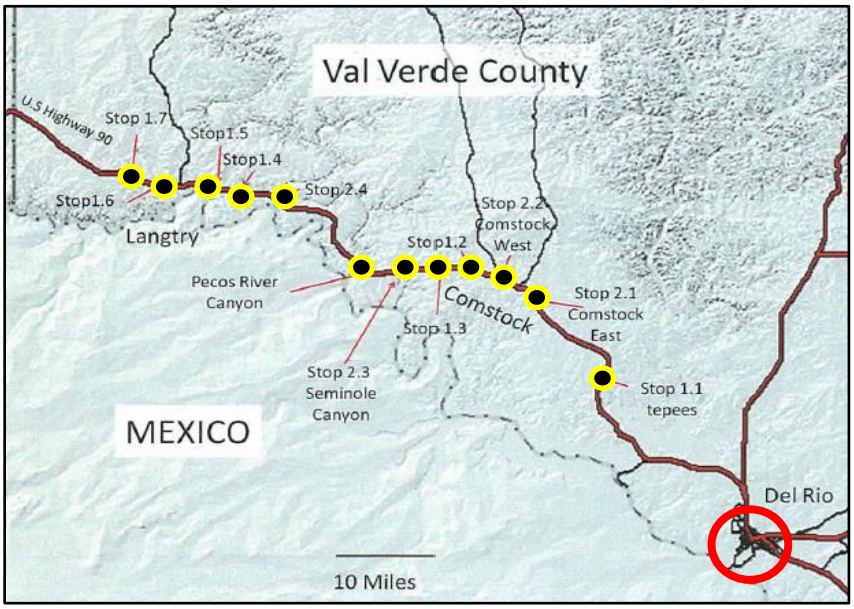

Figure 2 Locations of outcrops visited (Source: Lock et al. 2010)

Figure 3 shows the current hydrocarbon production from the Eagle Ford Formation, across the state of Texas. The green indicates the general area from which oil is being produced, yellow indicates wet gas/condensate production, red indicates gas production and black indicates the Eagle Ford Shale and the Austin Chalk outcrops. The red dot on the left of the figure indicates Val Verde County and the approximate location of the studied outcrops. Production is typically from 10,000 to 12,000 ft depth, and the subsurface formation averages about 250 ft thick (Lock et al., 2010).

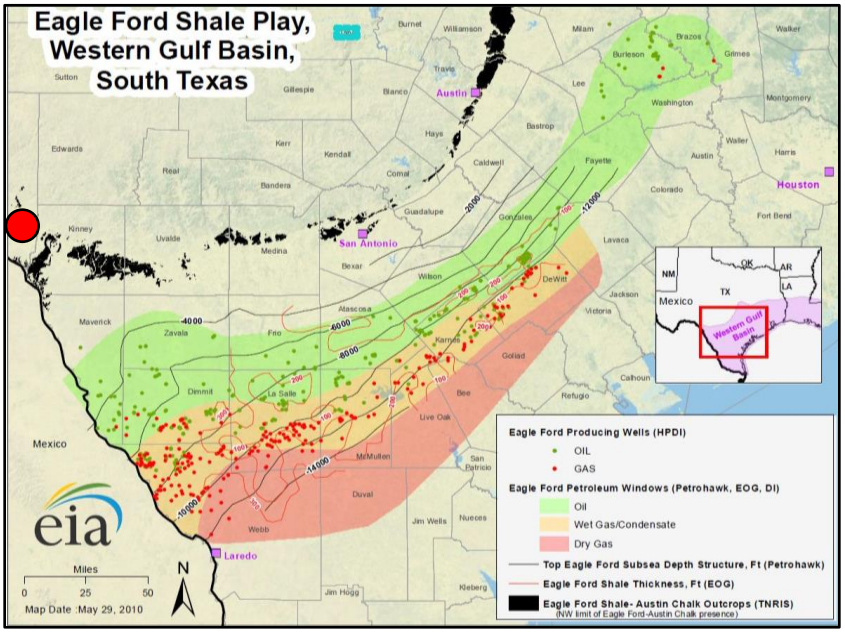

Figure 3 Map of Eagle Ford Formation across Texas (Source: U.S. Energy Information Administration).

The outcropping Eagle Ford (Boquillas) Formation can be informally divided into three members. The *lowest* member consists of unstable slope strata including debris flows, slump folds and breccias, possible turbidites, and contourites (Lock et al. 2010). Industry interest focuses primarily on the *middle* member, which can be further divided into: 1) lower beds comprising limestone-marlstone cycles that form a transgressive parasequence set with an upward decrease in the number of carbonate beds; 2) middle beds composed almost entirely of marlstones; and 3) upper beds ~~are~~ interpreted as a regressive parasequence set with increasing proportions of limestone towards the top (Lock et al. 2010). The middle member, where seen in an unweathered condition, consists of black, organic-rich strata that exudes a strong petroleum odor when broken. Fine laminations are undisturbed by bioturbation suggesting anaerobic and dysaerobic bottom water conditions during sedimentation.

The *upper* member is marked by several limestone beds at the base. The main part of the upper member contains abundant echinoids and is interpreted to represent a return to more normal, oxygenated water conditions. Thin ash beds occur throughout the formation, but to date have not been correlated.

Analytical studies of Eagle Ford (Boquillas) shale samples from the fresh outcrop include TOC (total organic carbon) values between 4.0% to 5.0%, porosity of approximately 10%, and permeability in the nanodarcy range (Lock et al., 2010).

CHAPTER 4

METHODS

In order to verify Equation 1, field and laboratory data were collected. Fracture density was measured in uniformly dipping sedimentary rocks in the Boquillas/Eagle Ford Formation, West of Del Rio, Texas. This area is the up-dip outcrop of an important unconventional reservoir in South Texas. In order to satisfy the assumption of constant strain, the measured layers must have no curvature and come from the same outcrop. Rock samples were then collected from each of those layers, and used to measure the material properties shown in Equation 1 at University of Texas at Arlington.

4.1 Field Work

The objective of the field work was to measure fracture density on the selected layers. Another objective of the field work was to collect rock samples for further study in the lab. The rock samples needed to be large enough for the acoustic tests to be conducted efficiently, as will be described in more detail the *Acoustic Testing* section of this report.

Figure 4 shows a part of one of the studied outcrops, with the Boquillas Formation in light grey at the bottom of the outcrop. This image represents ~~the~~ location "1-2", in the Lock et al. 2010 guidebook. Samples 2, 3, 4, 5 and 6 were collected from this location.

Figure 4 Guidebook Location "1-2" Outcrop

Figure 5 shows the general locations of the outcrops studied in this research. Appendix ABC contains more satellite images and detailed outcrop UTM locations.

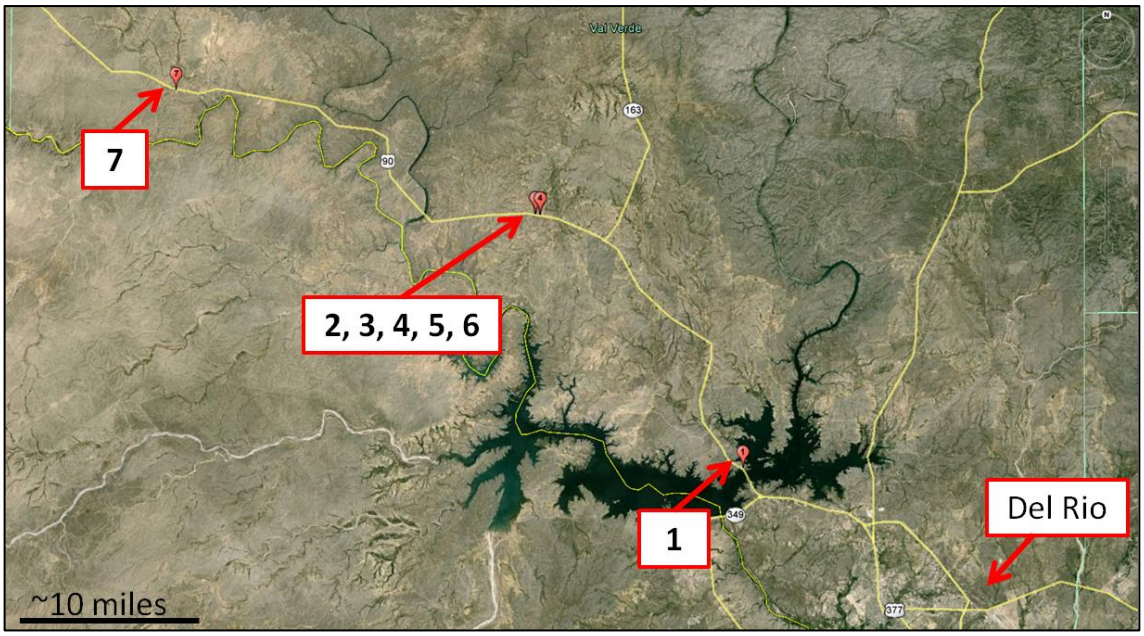

Figure 5 Satellite View of the Outcrops Studied. Locations of samples 1-7 noted. (Source: Google Earth)

Fracture density measurements can be obtained in a number of ways. The method used in this research is one described by Chiles et al. (2008), which entails measuring: (1) distances to fractures along scanlines on representative areas of a layer; (2) the fracture length of each fracture along the scanlines in the area; (3) fracture orientation; (4) thickness of the layer; (5) orientation of the layer; (6) orientation of the representative area containing the scanline; and (7) orientation of the scanlines (Chiles et al. 2008). These steps are followed in order to achieve accurate fracture density, using every factor that could affect the values. A number of scanlines, were used for every outcrop in order to collect the maximum number of data points and also to avoid sampling bias by relying on only one scanline. Figure 6 shows one such scanline being used to make fracture density measurements. Using a tape measure as scanline, the length and width of the area of interest were measured. Fractures crossing the

scanline were then counted, and their length and orientation measured. These values were later used in order to calculate the Measured Fracture Density.

One problem that could lead to inaccuracy in fracture density measurement data is the fact that the outcrops are road-cuts that have been created by blasting. The dynamite blasts generate their own fractures, which can usually be distinguished from the natural fractures. The solution to this problem was to measure only the regional joints, which is consistent with the assumption of Mode I extensional fractures used in Equation 1.

Figure 6 Scanline Method of Fracture Density Measurement

Figure 7 shows Sample 5, collected from Lock et al 2010 Guidebook Locality 1-2, approximately 31 miles West of Del Rio. This sample is of sufficient size for acoustic tests to be performed on it at the Geomechanics lab. The Boquillas Formation at the studied road-cuts have been exposed for many years, and weathered as a result. In certain cases, such as in samples 5, 6 and 7, once the samples are broken off of the outcrop, fresh, darker faces can be seen, which indicate the presence of hydrocarbon in the rock.

Figure 7 Example of the sample size collected.

4.2 Laboratory Work

Specimen density and elastic properties were measured in the laboratory. The *densities* were obtained using weight and volume measurements of the specimens. The *elastic* properties were obtained using dynamic tests. These acoustic velocity measurements were made by collaborators in the Geomechanics Laboratory of the Civil Engineering Department. Many of the samples were fragile, which made it difficult to collect large-enough samples for study in the lab. Three trips were made to the field in order to make enough fracture density measurements, and collect large samples for laboratory tests.

4.2.1 Sample Preparation

Samples collected in the field were cut to prepare two smooth sides for the acoustic tests to be carried out, and to measure the samples' densities. The samples underwent two cutting procedures, using two different saws. The first was done with a large saw (Figures 8 and 9). This saw was used to prepare the smooth sides needed for the acoustic testing.

Figure 8 Kerosene Saw, used to cut large samples.

Figure 9 Kerosene Saw, Sample Position.

The second and smaller saw (Figure 10), was used after the acoustic measurements were made. The samples were then cut into smaller pieces (Figure 11), in order to measure rock density.

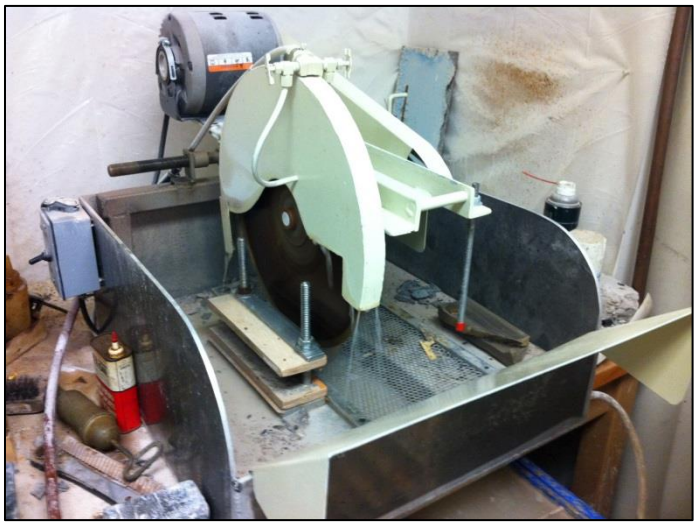

Figure 10 Water Saw, used to cut smaller samples

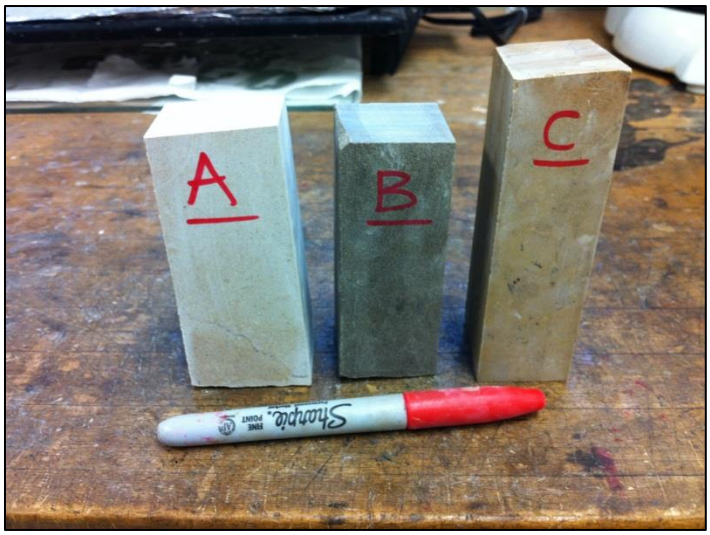

Figure 11 Samples, cut into smaller pieces

4.2.2 Density Measurements

Using an electronic balance (Figure 12) and a graduated cylinder (Figure 13), the mass and volume of the samples were measured to calculate density.

Figure 12 Electronic Balance

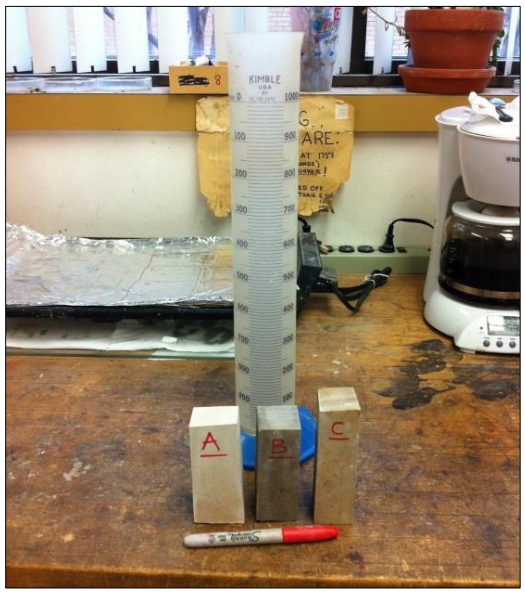

Figure 13 Graduated Cylinder

4.2.3 Acoustic Velocity Measurements

The test procedure followed ASTM standard 2000. The test setup is shown in Figure 14 and included an ultrasonic pulser/receiver (Model 5077PR, Olympus), a PC oscilloscope (PicoScope 5023, pico technology), and ultrasonic transducers (V101-RB and V150-RB, Olympus for p-wave and s-wave separately). The ultrasonic transducers were attached to the rock surface using the Panametrics-NDT SWC, a couplant to facilitate the transmission of sound energy between the transducer and the rock sample. A transducer pair was positioned onto the sample on opposite surfaces to measure the transit time of an ultrasonic pulse using through-transmission mode. Grease marks left on the rock sample surface (Figure 15) were from the couplant (Civil Engineering Geomechanics Lab, Dr. Xinbao Yu).

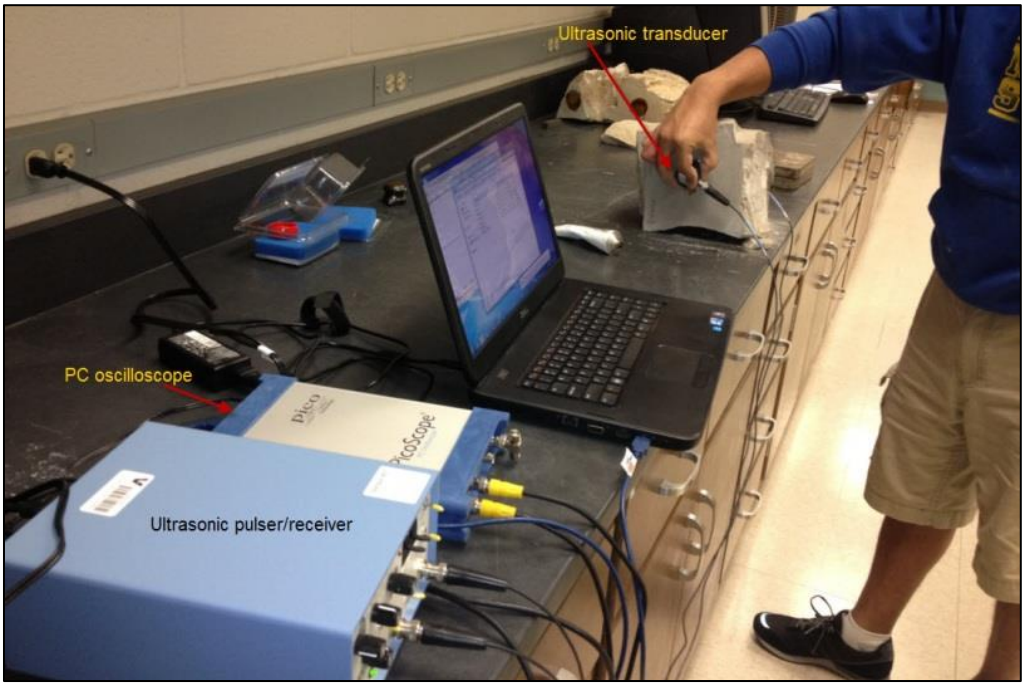

Figure 14 Acoustic Measurements Equipment Set-up

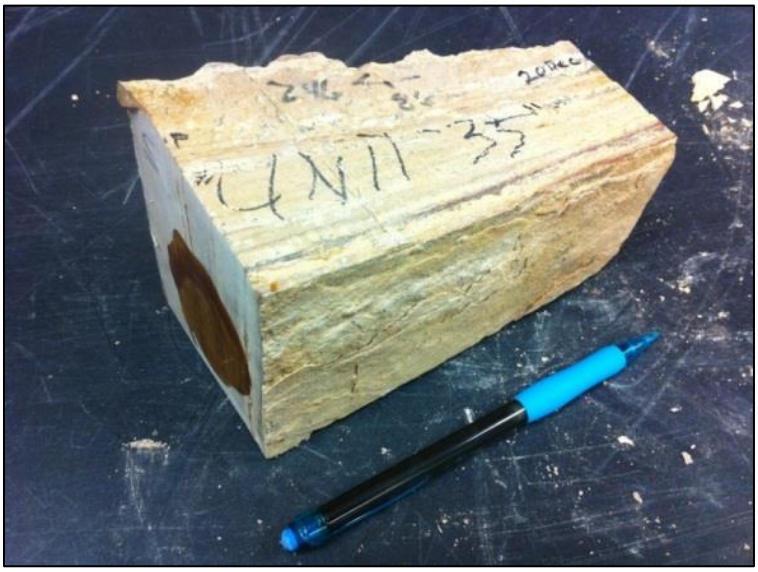

Figure 15 Sample prepared for acoustic tests

CHAPTER 5

RESULTS

The purpose of this study was to measure fracture density and associated material properties, in order to test Equation 1. The data presented in this section, as well as the supporting data in the Appendix, were used to test Equation 1.

5.1 Field Data

The appropriate data were collected during three field trips to Boquillas Formation outcrops in South Texas. Table 2 shows the data collected in the field, some of which were used to calculate Fracture Density and Critical Stress Intensity factors. The data for the 7 sites studied can be found in the Appendix, Tables A-B. Samples collected from each site were used to measure acoustic properties and density.

Table 2 List of some of the data collected in the field.

Data Collected in the Field
Date
Location
Station
UTM Coordinates
Strike of Outcrop (Right Hand Rule)
Dip of Outcrop (Right Hand Rule)
Thickness of Bed
Strike of Bed (Right Hand Rule)
Dip of Bed (Right Hand Rule)
Rock Description
Length of Sample Area
Width of Sample Area
Sample Orientation (Right Hand Rule)
Bed Curvature
Rake of Scanline (Bearing)
Elevation
Fracture Interval along scanline (feet)
Fracture Distance along scanline (Meters) Cumulative
Fracture Interval along scanline (Meters)
Fracture Length (inches)
Fracture Length (Meters)
Fracture Strike
Fracture Dip

5.2 Laboratory Data

The samples collected from each layer where fracture density was measured were then used to obtain density and acoustic measurements in the laboratory.

5.2.1 Density Measurements

In order to calculate densities, weight and volume of each sample were measured (Table 3). Those values were used to calculate the dry and saturated density of each sample as well as porosity (Table 4).

Table 3 Weight and Volume Measurements

Sample Number	Dry Weight (g)	Saturated Weight (g)	Weight Change (g)	Weight Change (%)	Volume (ml)
1	361.83	367.11	5.28	1.46	140
2	348.56	358.25	9.69	2.78	140
3	377.35	385.63	8.28	2.19	150
4	293.8	296.91	3.11	1.06	110
5	147.38	151.94	4.56	3.09	65
6	205.51	212.49	6.98	3.40	90
7	221.03	221.57	0.54	0.24	90

Table 4 Density Calculations

Sample Number	Density, Dry (g/ml)	Density, Saturated (g/ml)	Porosity (%)
1	2.58	2.62	3.77
2	2.49	2.56	6.92
3	2.52	2.57	5.52
4	2.67	2.70	2.83
5	2.27	2.34	7.02
6	2.28	2.36	7.76
7	2.46	2.46	0.60

5.2.2 Acoustic Measurements

In order to calculate the dynamic Young's Modulus, the Shear Modulus and Poisson's Ratio, P and S wave velocities were measured. Table 5 shows the results of the acoustic tests conducted in the Geomechanics Lab, at the Civil Engineering Department.

Table 5 Acoustic Tests Measurement Results

Sample #	Length (mm)	Travel Time (us)		Wave Velocity (m/s)		Wave Velocity (ft/s)	
		p-wave	s-wave	p-wave	s-wave	p-wave	s-wave
1	146.66	28.07	53.96	5224.8	2717.9	17141.73	8917.126
2	194.12	43.56	77.44	4456.38	2506.7	14620.67	8224.147
3	154.66	34.26	70.38	4514.3	2197.5	14810.69	7209.646
4	143.65	22	49	6529.5	2931.6	21422.25	9618.111
6	222.7	30	67	7423.3	3323.8	24354.66	10904.85
5	228.69	48	92	4764.3	2485.7	15630.91	8155.184
7	207.12	47	96	4406.8	2157.5	14458	7078.412

5.3 Calculations

Using the field and laboratory measurements, Fracture Density and material properties were calculated.

5.3.1 Fracture Density Calculations

Table 6 shows the Measured Fracture Density values, obtained using the field measurement values. Fracture density was calculated by dividing the sum of fracture lengths by the outcrop area. The fracture lengths were adjusted by a weighting factor to correct for potential bias caused as a result of fractures not being perpendicular to the surface of measurement or the scanline.

Table 6 Calculated Fracture Density

Sample	Fracture Density
1	0.3632
2	3.6005
3	1.3739
4	0.7647
5	0.8433
6	0.5345
7	1.2028

5.3.2 Plots of Equation 1

The purpose of this section of the study is to verify Equation 1, by plotting Equation 1, which assumes each measured layer had the same strain invariants. Equation 1 should plot as a straight line if it is valid. Samples 2, 3, 4, 5 and 6 have been collected from the guidebook location 1-2, in Lock et al.'s 2010 guidebook, sample 7 was collected from the guidebook location 1-5, and sample 1 from a location approximately 7 miles prior to guidebook location 1-1.

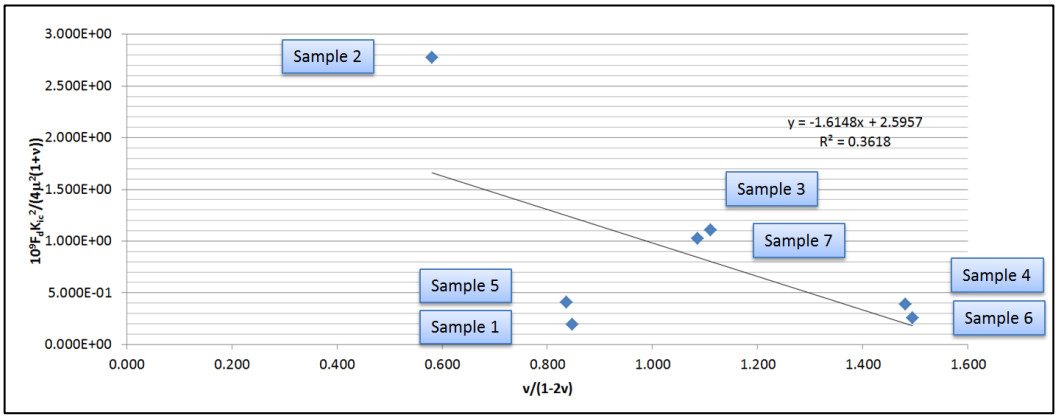

Figure 16 Plot of equation 1, with all 7 samples plotted, showing a correlation of 36.2%

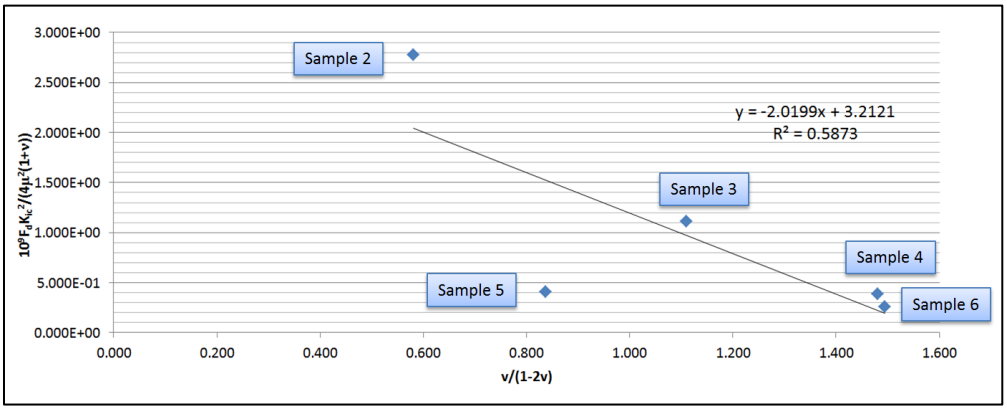

Figure 17 Plot of equation 1, having removed samples 1 and 7, due to their large distance from the rest of the samples produces this plot, with the correlation increased to 58.7%

Figure 18 shows the relationship between Uniaxial Extension and Fracture Density. This relationship can be interpreted as an estimation of comparative brittleness. For example, samples 4 and 6 have almost twice the fracture density as samples 3 and 7 for the same amount of uniaxial strain.

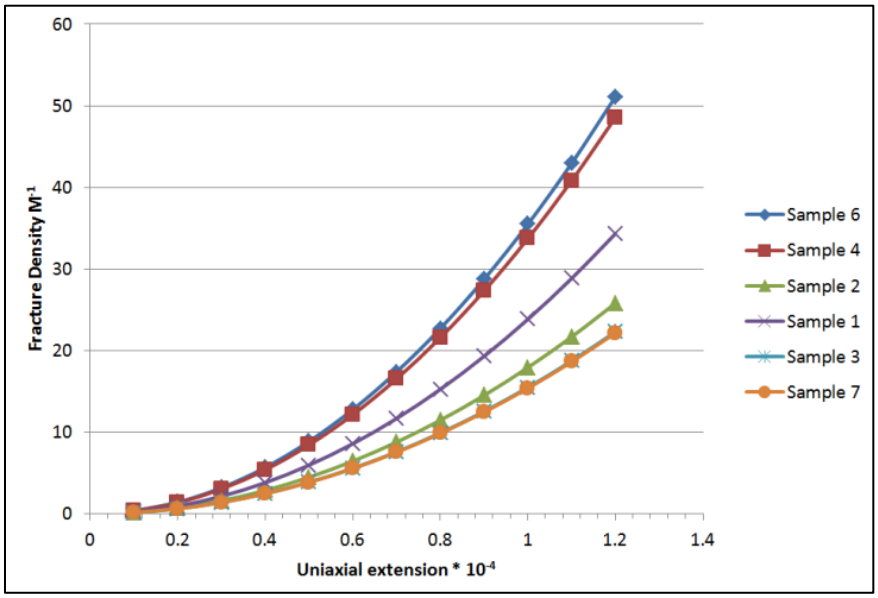

Figure 18 Uniaxial Extension vs. Fracture Density

CHAPTER 6

CONCLUSION

The purpose of this study was to verify the hypothesis that fracture density can be predicted under constant strain conditions using the elastic properties, rock density and fracture toughness. The hypothesis was framed in the form of Equation 1, the validity of which was tested. In order for the equation to be verified, the plot in Figure 16 needed to be a straight line, with a positive slope and a high correlation coefficient. The negative slope and the 58% correlation are evidence that the equation could not be confirmed in this study. There are two potential reasons for the poor correlation and negative slope of the line. One reason is the large spatial distance between samples. While samples 2, 3, 4, 5 and 6 were collected from the same guidebook outcrop, sample 1 was collected approximately 22 miles East of the large sample cluster, and sample 7 was collected approximately 26 miles West of the cluster. The second reason is the assumption of constant strain in the outcrops is not valid.

Further research, using the lessons learned from this study, on both macro- and micro-fracture level, on the same as well as different outcrops and formations could result in Equation 1, or a variation of it, to be verified.

APPENDIX A

FIELD DATA

Table 7

Sample #	Guidebook Location	Latitude, Longitude Coordinates
Sample 1	Not in the guidebook	29° 29' 31.04" N, 101° 2' 12.77" W
Sample 2	Loc 1-2, Anticline 1	29° 42' 34.46" N, 101° 14' 13.01" W
Sample 3	Loc 1-3	29° 42' 35.97" N, 101° 14' 27.19" W
Sample 4	Loc 1-2A, Anticline 1	29° 42' 35.01" N, 101° 14' 11.09" W
Sample 5	Loc 1-2B, Anticline 2	29° 42' 37.29" N, 101° 14' 29.93" W
Sample 6	Loc 1-2, Anticline 1	29° 42' 35.54" N , 101° 14' 13.91" W
Sample 7	Loc 1-5	29° 49' 0.46" N, 101° 35' 47.89" W

Table 8

Sample 1 of 7	
Date	9/30/2012
Location	Guidebook Stop 1-2
Station	1
UTM Coordinates	NAD 83 - 14R - 0302533 - 3264222
Strike of Outcrop (Right Hand Rule)	293
Dip of Outcrop (Right Hand Rule)	6
Thickness of Bed	4.333
Strike of Bed (Right Hand Rule)	293
Dip of Bed (Right Hand Rule)	6
Rock Description	Lower K Limestone - Fossiliferous - Fine grained Limestone
Length of Sample Area	27.58
Width of Sample Area	17
Sample Orientation (Right Hand Rule)	S270 - D87
Bed Curvature	0 (Flat)
Rake of Scanline (Bearing)	35
Elevation	1150

Table 9

Scanline #1 - Rake/Bearing of Scanline: 35						
Fracture Intervals along scanline (ft)	**Fracture Distance along scanline (Meters) Cumulative**	**Fracture Intervals along scanline (Meters)**	**Fracture Length (inches)**	**Fracture Length (Meters)**	**Fracture Strike**	**Fracture Dip**
0.583	0.1776984	0.1776984	107	2.7178	140	78
3.417	1.2192	1.0415016	64	1.6256	100	90
5.5	2.8956	1.6764	203	5.1562	120	90
13.167	6.9089016	4.0133016	20	0.508	170	90
2.333	7.62	0.7110984	179	4.5466	140	90
5.5	9.2964	1.6764	151	3.8354	110	90
4.25	10.5918	1.2954	83	2.1082	154	88

Table 10

Scanline #2 - Rake/Bearing of Scanline: 130						
Fracture Interval along scanline (feet)	**Fracture Distance along scanline (Meters) Cumulative**	**Fracture Interval along scanline (Meters)**	**Fracture Length (inches)**	**Fracture Length (Meters)**	**Fracture Strike**	**Fracture Dip**
12	3.6576	3.6576	79	2.0066	70	90
1.9	4.23672	0.57912	102	2.5908	72	90

Table 11

Scanline #3 - Rake/Bearing of Scanline: 35						
Fracture Interval along scanline (feet)	**Fracture Distance along scanline (Meters) Cumulative**	**Fracture Interval along scanline (Meters)**	**Fracture Length (inches)**	**Fracture Length (Meters)**	**Fracture Strike**	**Fracture Dip**
2.667	0.8129016	0.8129016	75	1.905	132	80
1.25	1.1939016	0.381	177	4.4958	310	90
2.75	2.0321016	0.8382	143	3.6322	165	90

Table 12

Scanline #4 - Rake/Bearing of Scanline: 130						
Fracture Interval along scanline (feet)	**Fracture Distance along scanline (Meters) Cumulative**	**Fracture Interval along scanline (Meters)**	**Fracture Length (inches)**	**Fracture Length (Meters)**	**Fracture Strike**	**Fracture Dip**
0.667	0.2033016	0.2033016	131	3.3274	2	90
17	5.3849016	5.1816	74	1.8796	110	90
7.417	7.6456032	2.2607016	131	3.3274	85	90
4.417	8.9919048	1.3463016	31	0.7874	63	90

Table 13

Sample 2 of 7	
Date	9/30/2012
Location	Guidebook Stop 1-4
Station	2
UTM Coordinates	NAD 83 - 14R - 0299668 - 3274519
Strike of Outcrop (Right Hand Rule)	15
Dip of Outcrop (Right Hand Rule)	90
Thickness of Bed	9
Strike of Bed (Right Hand Rule)	28
Dip of Bed (Right Hand Rule)	7
Rock Description	Limestone
Length of Sample Area	22
Width of Sample Area	9
Sample Orientation (Right Hand Rule)	Strike: 25, Dip: 89
Bed Curvature	0 (Flat)
Rake of Scanline (Bearing)	0
Elevation	1349

Table 14

Fracture Distance along scanline (ft)	Fracture Distance along scanline (Meters) Cumulative	Fracture Interval along scanline (Meters)	Fracture Length (inches)	Fracture Length (Meters)	Fracture Strike	Fracture Dip
1.25	0.381	0.381	7	0.1778	69	89
4	1.2192	0.8382	9.5	0.2413	60	86
4.916	1.4983968	0.2791968	9.5	0.2413	65	86
5.167	1.5749016	0.0765048	9.5	0.2413	65	86
5.333	1.6254984	0.0505968	9.5	0.2413	65	86
5.417	1.6511016	0.0256032	9.5	0.2413	65	86
5.667	1.7273016	0.0762	9.5	0.2413	317	86
8.5	2.5908	0.8634984	9.5	0.2413	51	87
9	2.7432	0.1524	9.5	0.2413	255	90
10.333	3.1494984	0.4062984	9.5	0.2413	267	90
11.25	3.429	0.2795016	9.5	0.2413	280	90
11.75	3.5814	0.1524	9.5	0.2413	240	90
13.583	4.1400984	0.5586984	9.5	0.2413	248	90
14.333	4.3686984	0.2286	9.5	0.2413	330	90
14.667	4.4705016	0.1018032	9.5	0.2413	243	90
15.5	4.7244	0.2538984	9.5	0.2413	252	90
17.67	5.385816	0.661416	9.5	0.2413	250	90

Table 15

Sample 3 of 7	
Date	9/30/2012
Location	Guidebook Stop 1-4
Station	3
UTM Coordinates	NAD83 - 14R - 0299668 - 3274519
Strike of Outcrop (Right Hand Rule)	15
Dip of Outcrop (Right Hand Rule)	90
Thickness of Bed	32"
Strike of Bed (Right Hand Rule)	28
Dip of Bed (Right Hand Rule)	7
Rock Description	Limey Shales
Length of Sample Area	17
Width of Sample Area	32
Sample Orientation (Right Hand Rule)	Strike: 5, Dip: 2
Bed Curvature	0 (Flat)
Rake of Scanline (Bearing)	0
Elevation	1349 14R

Table 16

Fracture Distance along scanline	Fracture Distance along scanline (Meters) Cumulative	Fracture Interval along scanline (Meters)	Fracture Length (inches)	Fracture Length (Meters)	Fracture Strike	Fracture Dip
1.167	0.3557016	0.3556	23	0.58	285	90
3.833	1.1682984	0.8125968	5	0.13	285	90
6.583	2.0064984	0.8382	32	0.81	308	90
7	2.1336	0.1271016	22	0.56	305	90
8.75	2.667	0.5334	6	0.15	330	90
9.583	2.9208984	0.2538984	14.5	0.37	303	90
9.797	2.9861256	0.0652272	13	0.33	295	90
9.833	2.9970984	0.0109728	10	0.25	255	90
12.333	3.7590984	0.762	2	0.05	245	90
15.5	4.7244	0.9653016	13	0.33	295	90
15.667	4.7753016	0.0509016	29	0.74	290	90
17.75	5.4102	0.6348984	11.5	0.29	255	90
18.333	5.5878984	0.1776984	29	0.74	300	90
18.667	5.6897016	0.1018032	27	0.69	277	90

Table 17

Sample 4 of 7	
Date	4/30/2013
Location	Guidebook Stop 1-2
Station	4
UTM Coordinates	NAD83 - 14R - 0283650 - 3288717
Strike of Outcrop (Right Hand Rule)	290
Dip of Outcrop (Right Hand Rule)	90
Thickness of Bed	1.75
Strike of Bed (Right Hand Rule)	110
Dip of Bed (Right Hand Rule)	6
Rock Description	Carbonate Siltstone
Length of Sample Area	27
Width of Sample Area	1.75
Sample Orientation (Right Hand Rule)	
Bed Curvature	0 (Flat)
Rake of Scanline (Bearing)	0
Elevation	1150

Table 18

Fracture Distance along scanline	Fracture Distance along scanline (Meters) Cumulative	Fracture Interval along scanline (Meters)	Fracture Length (inches)	Fracture Length (Meters)	Fracture Strike	Fracture Dip
2.25	0.6858	0.6858	1.75	0.5334	150	82
11.166	3.4033968	2.7175968	1.75	0.5334	140	75
18.25	5.5626	2.1592032	1.75	0.5334	205	68
25.75	7.8486	2.286	1.75	0.5334	140	81

Table 19

Sample 5 of 7	
Date	4/31/2013
Location	Guidebook Stop 1-4
Station	6
UTM Coordinates	NAD83 - 14R - 0283145 - 3288797
Strike of Outcrop (Right Hand Rule)	280
Dip of Outcrop (Right Hand Rule)	90
Thickness of Bed	5"
Strike of Bed (Right Hand Rule)	100
Dip of Bed (Right Hand Rule)	6
Rock Description	
Length of Sample Area	22.667
Width of Sample Area	0.417
Sample Orientation (Right Hand Rule)	
Bed Curvature	0 (Flat)
Rake of Scanline (Bearing)	0
Elevation	1349

Table 20

Fracture Distance along scanline	Fracture Distance along scanline (Meters) Cumulative	Fracture Interval along scanline (Meters)	Fracture Length (inches)	Fracture Length (Meters)	Fracture Strike	Fracture Dip
0.917	0.2795016	0.2795016	0.33	0.100584	125	83
3.25	0.9906	0.7110984	0.417	0.1271016	145	90
11.333	3.4542984	2.4636984	0.417	0.1271016	150	85
20.75	6.3246	2.8703016	0.417	0.1271016	150	84

Table 21

Sample 6 of 7	
Date	4/30/2013
Location	Guidebook Stop 1-2
Station	5
UTM Coordinates	NAD83 - 14R - 0283598 - 3288710
Strike of Outcrop (Right Hand Rule)	290
Dip of Outcrop (Right Hand Rule)	90
Thickness of Bed	4.25
Strike of Bed (Right Hand Rule)	190
Dip of Bed (Right Hand Rule)	6
Rock Description	Carbonate Siltstone
Length of Sample Area	27
Width of Sample Area	4.25
Sample Orientation (Right Hand Rule)	
Bed Curvature	0 (Flat)
Rake of Scanline (Bearing)	0
Elevation	1150

Table 22

Fracture Distance along scanline	Fracture Distance along scanline (Meters) Cumulative	Fracture Interval along scanline (Meters)	Fracture Length (inches)	Fracture Length (Meters)	Fracture Strike	Fracture Dip
0.5	0.1524	1.8288	4.083	1.2444984	165	80
8.167	2.4893016	2.3369016	4.25	1.2954	190	90
16.333	4.9782984	2.4889968	4.25	1.2954	170	90
26.917	8.2043016	3.2260032	4.25	1.2954	180	90

Table 23

Sample 7 of 7	
Date	4/31/2013
Location	Guidebook Stop 1-5
Station	7
UTM Coordinates	NAD83 - 14R - 0249058 - 3301318
Strike of Outcrop (Right Hand Rule)	280
Dip of Outcrop (Right Hand Rule)	90
Thickness of Bed	2.25
Strike of Bed (Right Hand Rule)	100
Dip of Bed (Right Hand Rule)	7
Rock Description	
Length of Sample Area	19
Width of Sample Area	2.25
Sample Orientation (Right Hand Rule)	
Bed Curvature	0 (Flat)
Rake of Scanline (Bearing)	0
Elevation	

Table 24

Fracture Distance along scanline	Fracture Distance along scanline (Meters) Cumulative	Fracture Interval along scanline (Meters)	Fracture Length (inches)	Fracture Length (Meters)	Fracture Strike	Fracture Dip
0.500	0.152	0.152	1.500	0.457	195.000	87.000
1.500	0.457	0.305	2.250	0.686	210.000	85.000
4.083	1.245	0.787	2.250	0.686	205.000	84.000
4.833	1.473	0.229	2.250	0.686	210.000	86.000
8.417	2.566	2.566	2.250	0.686	200.000	85.000
15.000	4.572	2.006	2.250	0.686	200.000	90.000
18.667	5.690	1.118	2.250	0.686	165.000	90.000

APPENDIX B

LABORATORY MEASUREMENTS

Table 25

Sample Number	Dry Weight (g)	Saturated Weight (g)	Weight Change (g)	Weight Change (%)	Volume (ml)
1	361.83	367.11	5.28	1.46	140
2	348.56	358.25	9.69	2.78	140
3	377.35	385.63	8.28	2.19	150
4	293.8	296.91	3.11	1.06	110
5	147.38	151.94	4.56	3.09	65
6	205.51	212.49	6.98	3.40	90
7	221.03	221.57	0.54	0.24	90

Table 26

Sample Number	Density, Dry (g/ml)	Density, Saturated (g/ml)	Porosity (%)
1	2.585	2.622	3.7716
2	2.490	2.558	6.9216
3	2.516	2.570	5.520
4	2.671	2.699	2.827
5	2.267	2.338	7.015
6	2.283	2.361	7.756
7	2.456	2.462	0.600

Acoustic Measurements

Table 27

Rock Sample	Length (mm)	Travel Time (us)		Wave Velocity (m/s)		Wave Velocity (ft/s)	
		p-wave	s-wave	p-wave	s-wave	p-wave	s-wave
1	146.66	28.07	53.96	5224.8	2717.94	17141.733	8917.126
2	194.12	43.56	77.44	4456.38	2506.72	14620.670	8224.147
3	154.66	34.26	70.38	4514.3	2197.5	14810.696	7209.646
4	143.65	22	49	6529.5	2931.6	21422.245	9618.111
5	228.69	48	92	4764.3	2485.7	15630.906	8155.184
6	222.7	30	67	7423.3	3323.8	24354.660	10904.856
7	207.12	47	96	4406.8	2157.5	14458.006	7078.412

P- and S-wave Velocities

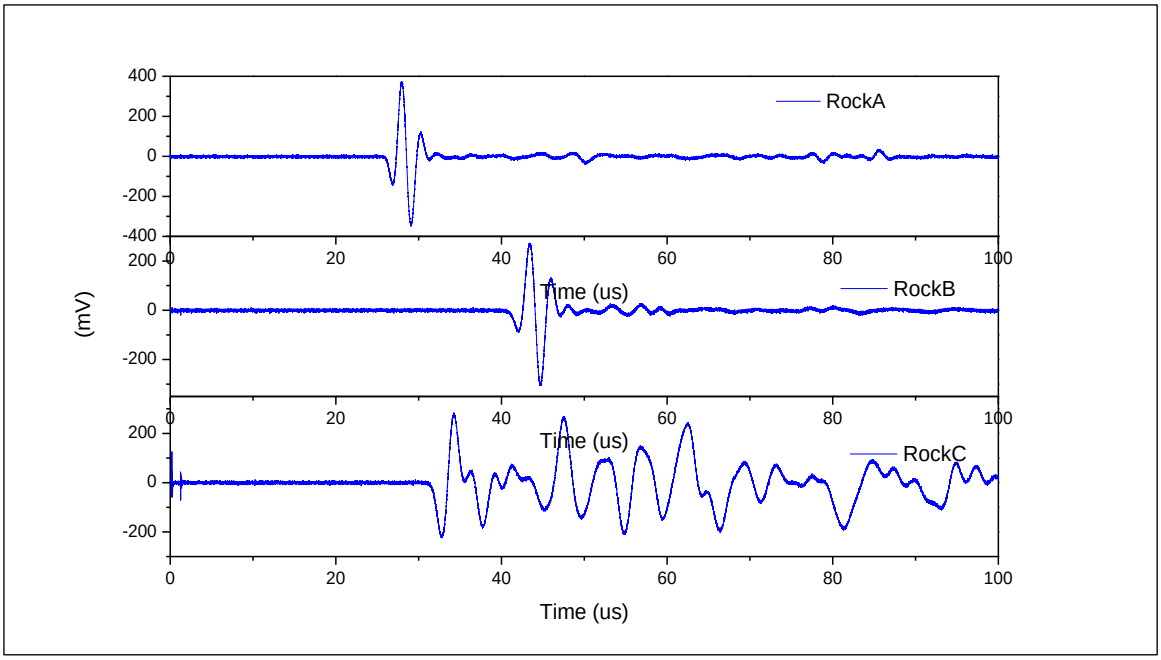

Figure 19 Samples 1-3, P-wave Signals

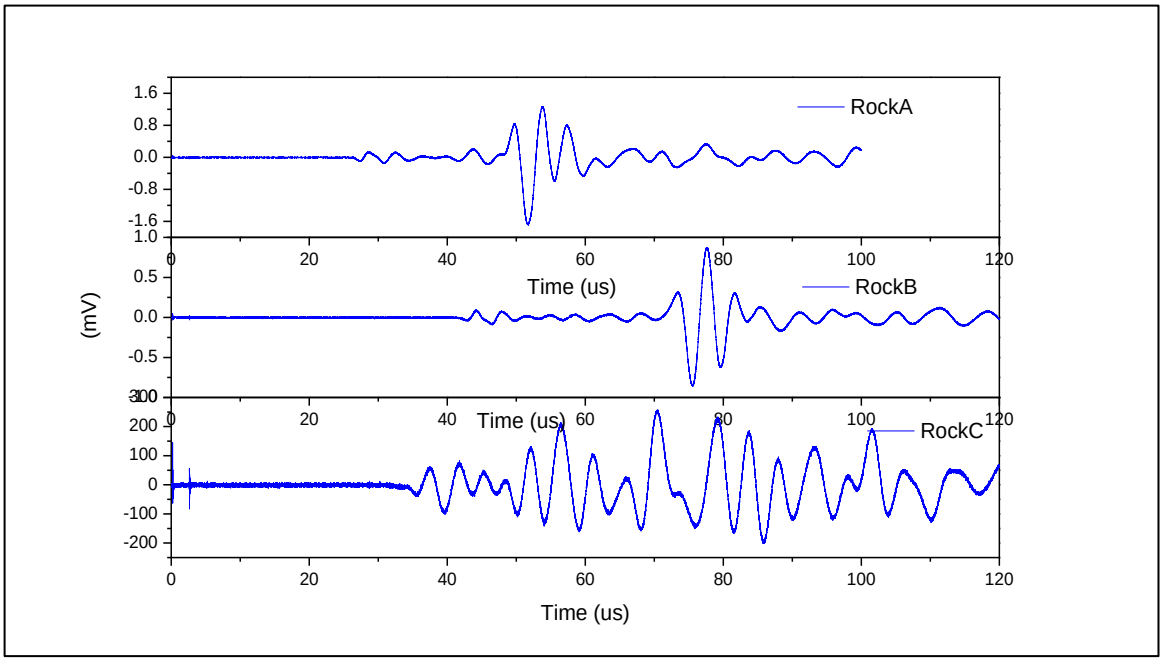

Figure 20 Samples 1-3, S-wave Signals

P-wave Signals, Samples 4-7

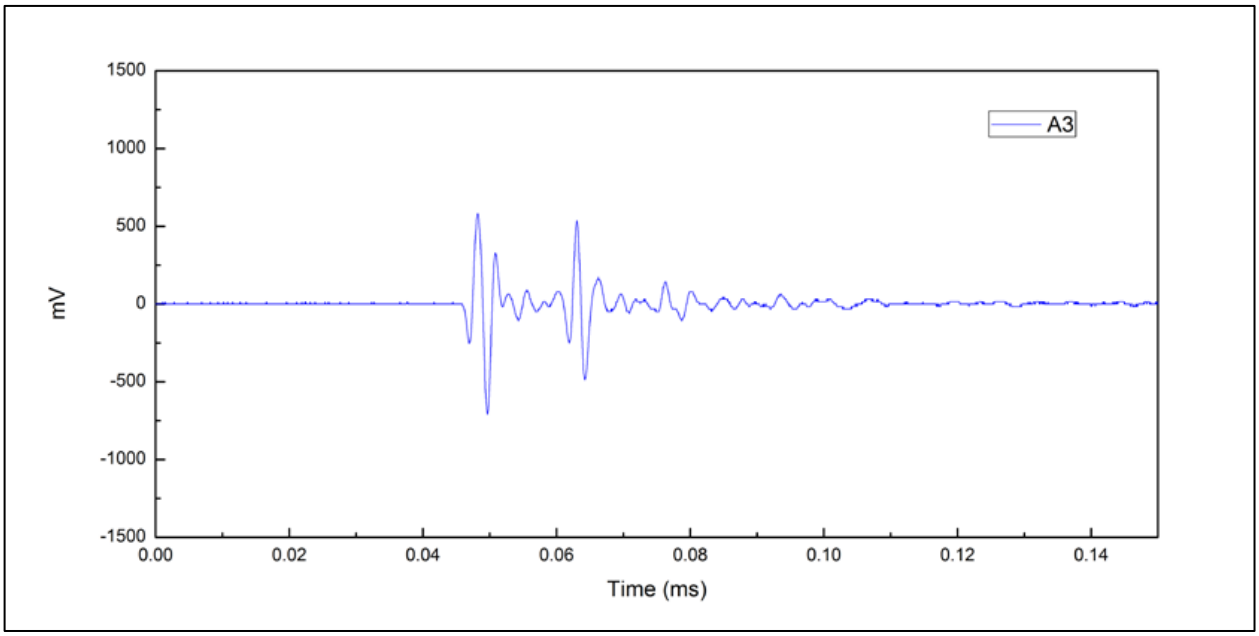

Figure 21 P-wave Signal, Sample 4

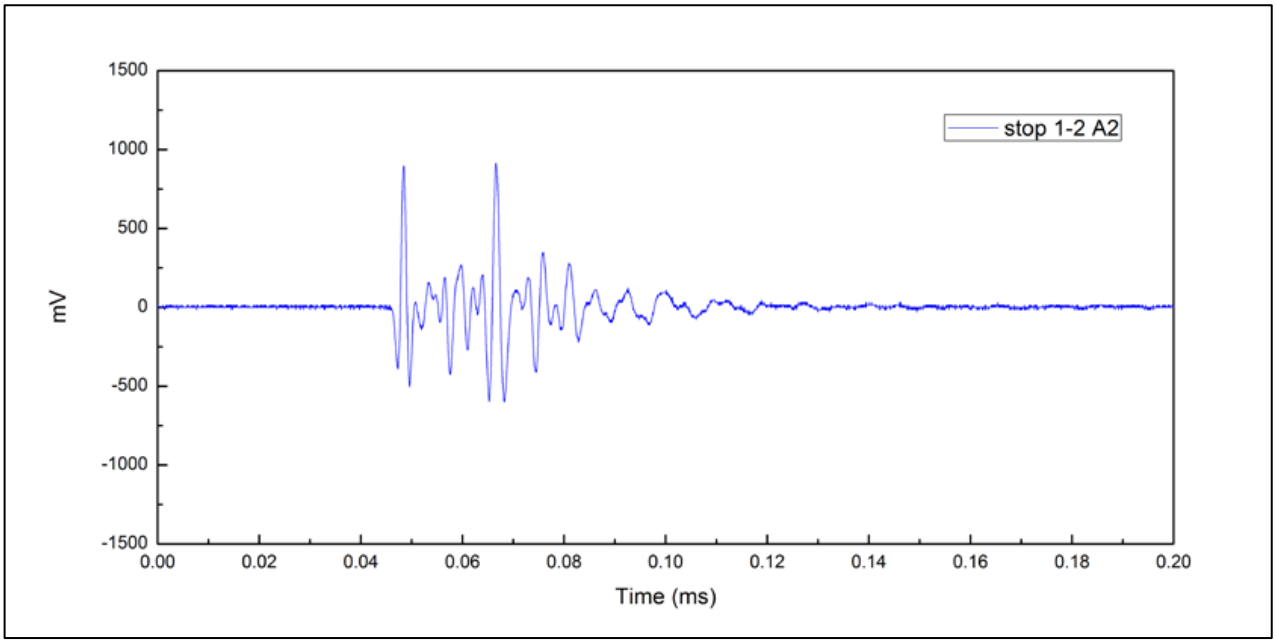

Figure 22 P-wave Signal, Sample 5

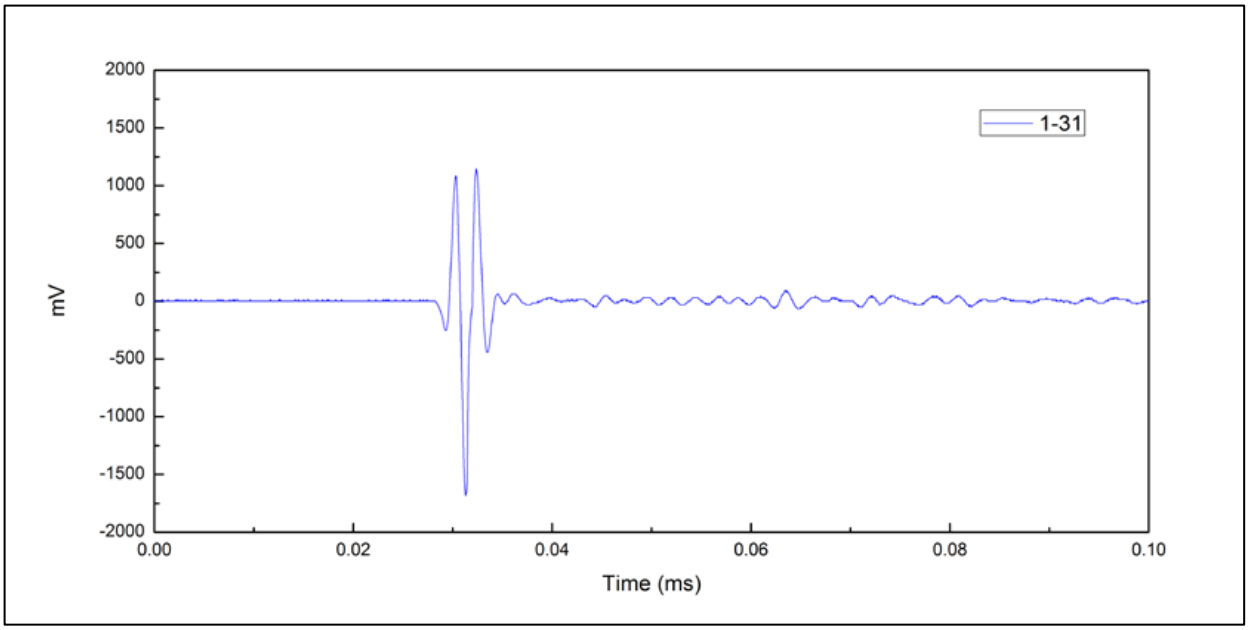

Figure 23 P-Wave Signal, Sample 6

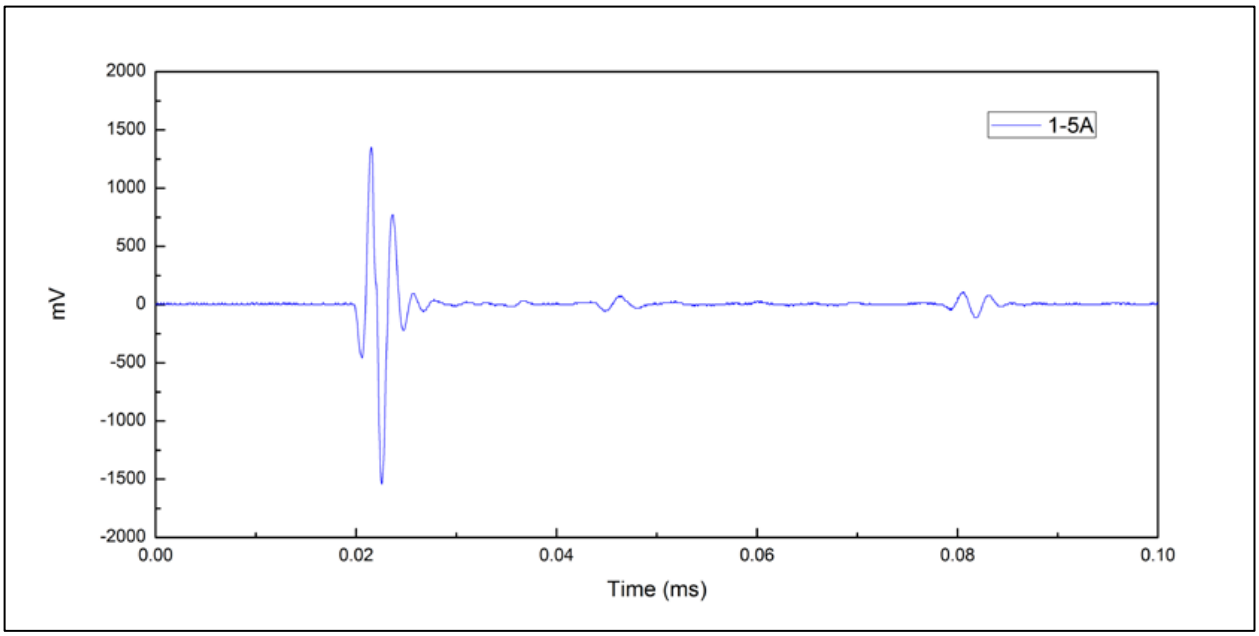

Figure 24 P-wave Signal, Sample 7

S-wave Signals, Samples 4-7

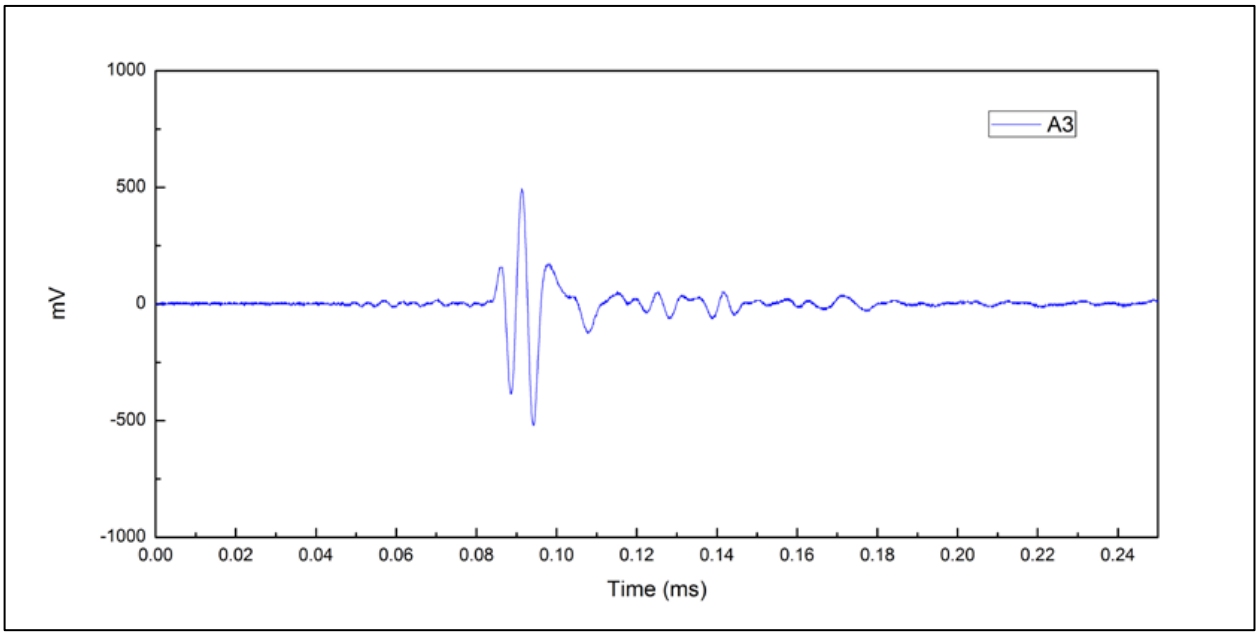

Figure 25 S-wave Signal, Sample 4

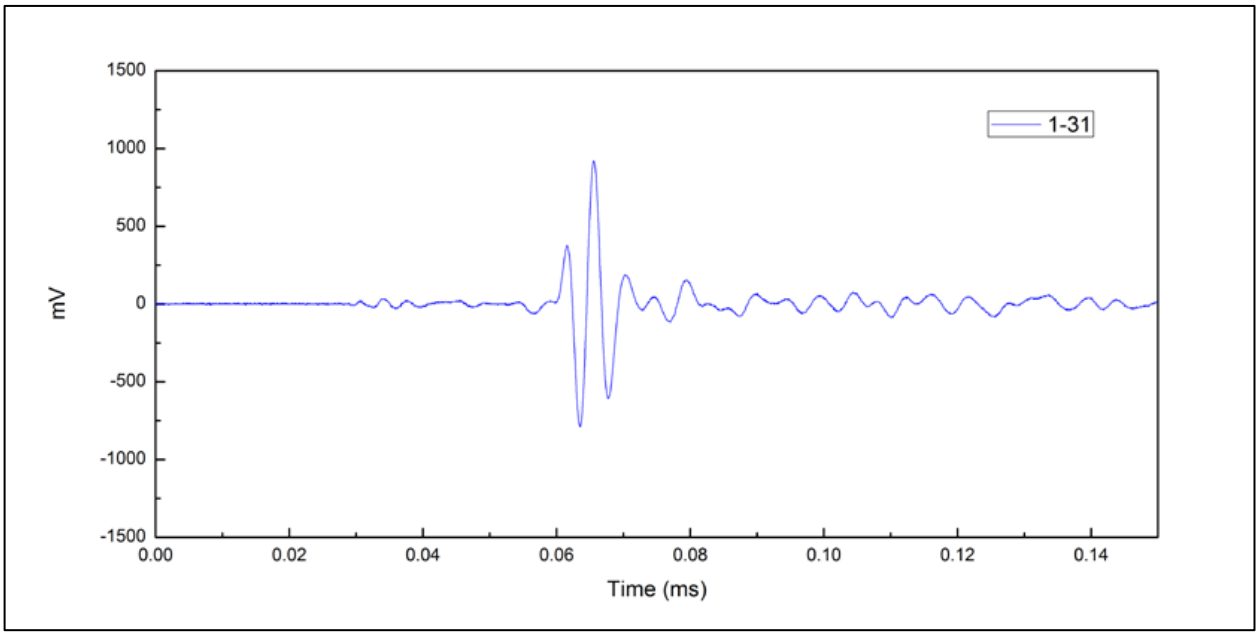

Figure 26 S-wave Signal, Sample 5

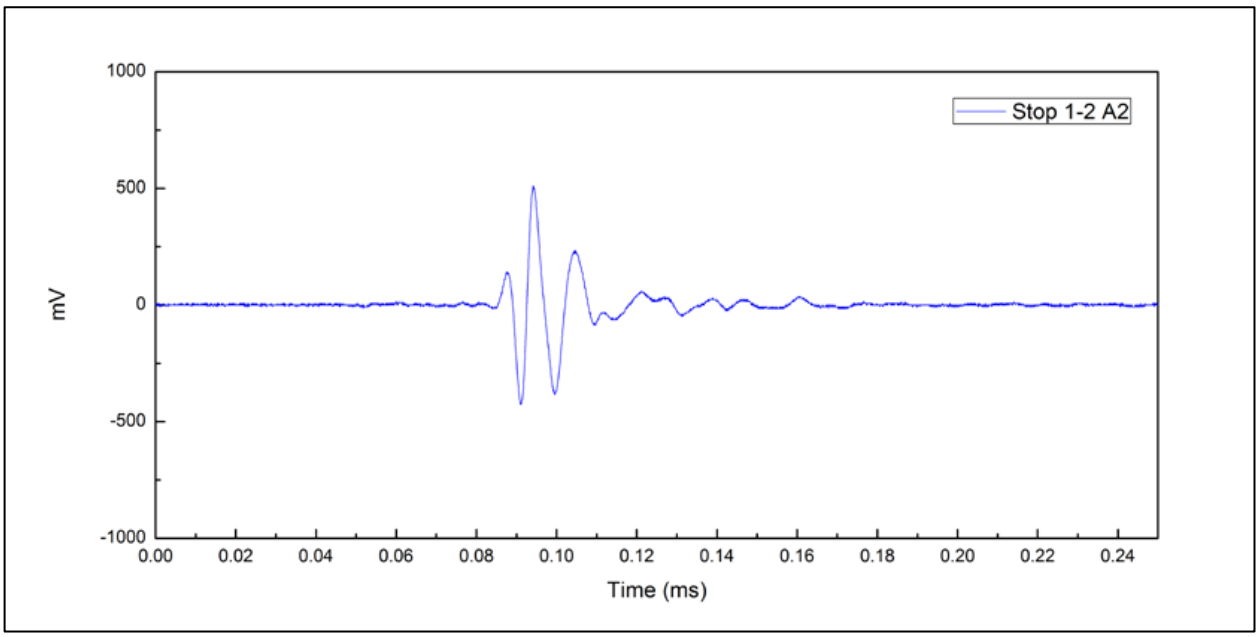

Figure 27 S-wave Signal, Sample 6

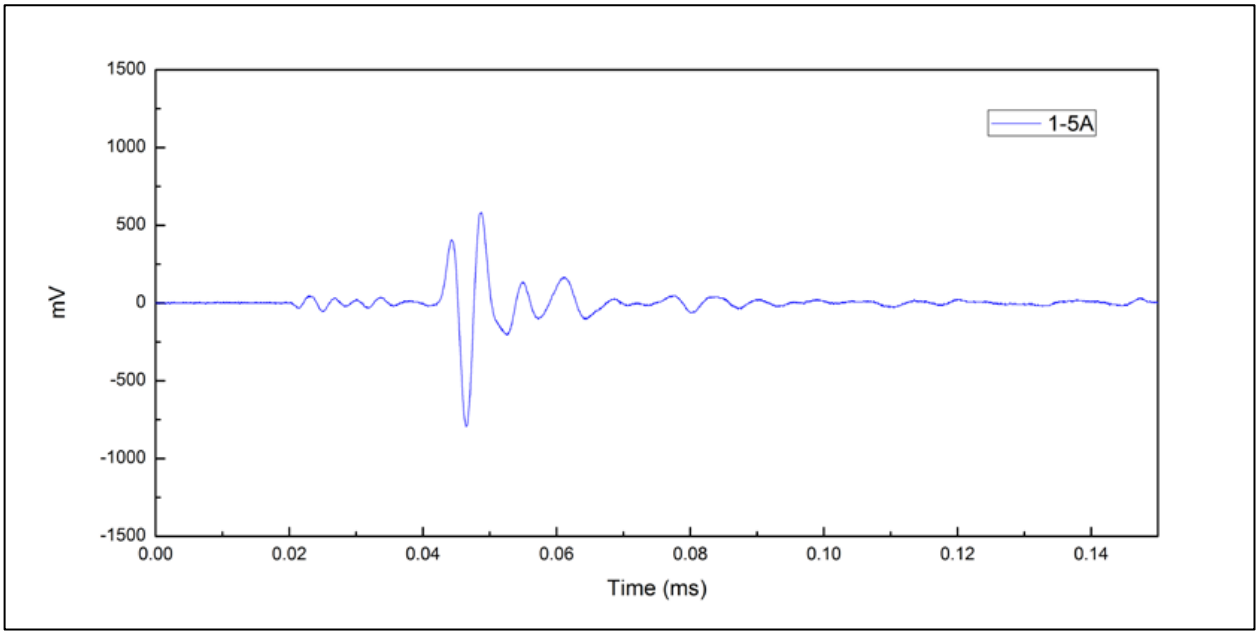

Figure 28 S-wave Signal, Sample 7

APPENDIX C

FRACTURE DENSITY CALCULATIONS

Table 28 Sample 1, Scan-line 1

Scan Line	Trend	Fracture Distance (M)	Fracture Length (M)	Fracture Strike	Fracture Dip	Fracture Vector x coord	Fracture Vector y coord	Fracture Vector z coord	Weighting factor for line length	Weighted Fracture Length	Cross product Fracture line length projection Vector (x)	Cross product Fracture line length projection Vector (y)	Cross product Fracture line length projection Vector (z)
1	35	0.178	2.7178	140	78	0.63	-0.75	0.21	0.99	2.736	0.75	0.65	0.05
1	35	1.219	1.6256	100	90	0.98	-0.17	0.00	0.99	1.634	0.17	0.98	-0.02
1	35	2.896	5.1562	120	90	0.87	-0.50	0.00	0.99	5.184	0.50	0.86	0.01
1	35	6.909	0.508	170	90	0.17	-0.98	0.00	1.00	0.509	0.98	0.17	0.09
1	35	7.620	4.5466	140	90	0.64	-0.77	0.00	1.00	4.566	0.76	0.64	0.05
1	35	9.296	3.8354	110	90	0.94	-0.34	0.00	0.99	3.856	0.34	0.93	-0.01
		10.592	2.1082	154	88	0.44	-0.90	0.03	1.00	2.110	0.89	0.44	0.07
		10.592					*Fracture Density Line 1 = 0.671*						

Table 29 Sample 1, Scan-line 2

Scan Line	Trend	Fracture Distance (M)	Fracture Length (M)	Fracture Strike	Fracture Dip	Fracture Vector x coord	Fracture Vector y coord	Fracture Vector z coord	Weighting factor for line length	Weighted Fracture Length	Cross product Fracture line length projection Vector (x)	Cross product Fracture line length projection Vector (y)	Cross product Fracture line length projection Vector (z)
2	130	3.6576	2.0066	70	90	0.939692621	0.342020143	0	0.997073625	2.012489298	-0.340146521	0.934544886	-0.071288241
2	130	4.2418	2.5908	72	90	0.951056516	0.309016994	0	0.996883435	2.598899639	-0.307324167	0.945846529	-0.068576842
		4.2418							Frac Density Line 2	0.1501319			

Table 30 Sample 1, Scan-line 3

Scan Line	Trend	Fracture Distance (M)	Fracture Length (M)	Fracture Strike	Fracture Dip	Fracture Vector x coord	Fracture Vector y coord	Fracture Vector z coord	Weighting factor for line length	Weighted Fracture Length	Cross product Fracture line length projection Vector (x)	Cross product Fracture line length projection Vector (y)	Cross product Fracture line length projection Vector (z)
3	130	0.8128	1.905	132	80	0.731854786	-0.658965009	0.17364818	0.997156028	1.910433218	0.66244736	0.744553855	0.033514129
3	130	1.1938	4.4958	310	90	-0.766044443	0.64278761	0	0.994991349	4.518431244	-0.639266352	-0.761847972	-0.030561165
3	130	2.032	3.6322	165	90	0.258819045	-0.965925826	0	0.997927123	3.639744742	0.960634384	0.257401207	0.082369553
		2.032							Frac Density Line 3	0.32780133			

Table 31 Sample 1, Scan-line 4

Scan Line	Trend	Fracture Distance (M)	Fracture Length (M)	Fracture Strike	Fracture Dip	Fracture Vector x coord	Fracture Vector y coord	Fracture Vector z coord	Weighting factor for line length	Weighted Fracture Length	Cross product Fracture line length projection Vector (x)	Cross product Fracture line length projection Vector (y)	Cross product Fracture line length projection Vector (z)
4	35	0.2032	3.3274	2	90	0.034899497	0.999390827	0	0.999298141	3.329737006	-0.993916060	0.034708314	-0.097585727
	35	5.3848	1.8796	110	90	0.939692621	-0.342020143	0	0.994536941	1.889924770	0.340146521	0.934544886	-0.005470597
	35	7.6454	3.3274	85	90	0.996194698	0.087155743	0	0.995731878	3.341662623	-0.086678294	0.990737439	-0.049073141
	35	8.9916	0.7874	63	90	0.891006524	0.4539905	0	0.997740225	0.789183376	-0.451503492	0.886125497	-0.080073448
		8.9916							Frac Density Line 4	0.304422272			

Sample 1, Average Fracture Density:

Average Frac Density	0.363227221

Table 32 Sample 2

Scan Line	Trend	Fracture Distance (M)	Fracture Length (M)	Fracture Strike	Fracture Dip	Fracture Vector x coord	Fracture Vector y coord	Fracture Vector z coord	Weighting factor for line length	Weighted Fracture Length	Cross product Fracture line length projection Vector (x)	Cross product Fracture line length projection Vector (y)	Cross product Fracture line length projection Vector (z)
1	15	0.381	0.1778	69	89	0.93	0.36	0.02	0.81	0.219755221	0.02	0.00	-0.81
1	15	1.2192	0.2413	60	86	0.86	0.50	0.07	0.71	0.340422496	0.07	-0.02	-0.71
1	15	1.4983968	0.2413	65	86	0.90	0.42	0.07	0.77	0.314456565	0.07	-0.02	-0.76
1	15	1.5749016	0.2413	65	86	0.90	0.42	0.07	0.77	0.314456565	0.07	-0.02	-0.76
1	15	1.6254984	0.2413	65	86	0.90	0.42	0.07	0.77	0.314456565	0.07	-0.02	-0.76
1	15	1.6511016	0.2413	65	86	0.90	0.42	0.07	0.77	0.314456565	0.07	-0.02	-0.76
1	15	1.7273016	0.2413	317	86	-0.68	0.73	0.07	0.85	0.284265828	0.07	-0.02	0.85
1	15	2.5908	0.2413	51	87	0.78	0.63	0.05	0.59	0.409463116	0.05	-0.01	-0.59
1	15	2.7432	0.2413	255	90	-0.97	-0.26	0.00	0.87	0.27862924	0.00	0.00	0.87
1	15	3.1494984	0.2413	267	90	-1.00	-0.05	0.00	0.95	0.253717835	0.00	0.00	0.95
1	15	3.429	0.2413	280	90	-0.98	0.17	0.00	1.00	0.242221727	0.00	0.00	1.00
1	15	3.5814	0.2413	240	90	-0.87	-0.50	0.00	0.71	0.341249	0.00	0.00	0.71

										733			
1	15	4.1400984	0.2413	248	90	-0.93	-0.37	0.00	0.80	0.302140334	0.00	0.00	0.80
1	15	4.3686984	0.2413	330	90	-0.50	0.87	0.00	0.71	0.341249733	0.00	0.00	0.71
1	15	4.4705016	0.2413	243	90	-0.89	-0.45	0.00	0.74	0.324701178	0.00	0.00	0.74
1	15	4.7244	0.2413	252	90	-0.95	-0.31	0.00	0.84	0.287717263	0.00	0.00	0.84
1	15	5.385816	0.2413	250	90	-0.94	-0.34	0.00	0.82	0.294572908	0.00	0.00	0.82
1	15	5.2830984	0.2413	330	90	-0.50	0.87	0.00	0.71	0.341249733	0.00	0.00	0.71
									Frac Density Line 1	3.600484066			

Table 33 Sample 3

Scan Line	Trend	Fracture Distance (M)	Fracture Length (M)	Fracture Strike	Fracture Dip	Fracture Vector x coord	Fracture Vector y coord	Fracture Vector z coord	Weighting factor for line length	Weighted Fracture Length	Cross product Fracture line length projection Vector (x)	Cross product Fracture line length projection Vector (y)	Cross product Fracture line length projection Vector (z)
1	15	0.3557016	0.5842	285	90	-0.97	0.26	0.00	1.00	0.5842	0.00	0.00	1.00
1	15	1.1682984	0.127	285	90	-0.97	0.26	0.00	1.00	0.127	0.00	0.00	1.00
1	15	2.0064984	0.8128	308	90	-0.79	0.62	0.00	0.92	0.882993715	0.00	0.00	0.92
1	15	2.1336	0.5588	305	90	-0.82	0.57	0.00	0.94	0.594662539	0.00	0.00	0.94
1	15	2.667	0.1524	330	90	-0.50	0.87	0.00	0.71	0.215526147	0.00	0.00	0.71
1	15	2.9208984	0.3683	303	90	-0.84	0.54	0.00	0.95	0.387253537	0.00	0.00	0.95
1	15	2.9861256	0.3302	295	90	-0.91	0.42	0.00	0.98	0.335293867	0.00	0.00	0.98
1	15	2.9970984	0.254	255	90	-0.97	-0.26	0.00	0.87	0.293293937	0.00	0.00	0.87
1	15	3.7590984	0.0508	245	90	-0.91	-0.42	0.00	0.77	0.06631469	0.00	0.00	0.77
1	15	4.7244	0.3302	295	90	-0.91	0.42	0.00	0.98	0.335293867	0.00	0.00	0.98
1	15	4.7753016	0.7366	290	90	-0.94	0.34	0.00	1.00	0.739413692	0.00	0.00	1.00
1	15	5.4102	0.2921	255	90	-0.97	-0.26	0.00	0.87	0.337288	0.00	0.00	0.87

										027			
1	15	5.5878984	0.7366	300	90	-0.87	0.50	0.00	0.97	0.762584434	0.00	0.00	0.97
1	15	5.6897016	0.6858	277	90	-0.99	0.12	0.00	0.99	0.692539749	0.00	0.00	0.99
		5.6897016							Frac Density Line 1	1.373885889			

Table 34 Sample 4

Scan Line	Trend	Fracture Distance (M)	Fracture Length (M)	Fracture Strike	Fracture Dip	Fracture Vector x coord	Fracture Vector y coord	Fracture Vector z coord	Weighting factor for line length	Weighted Fracture Length	Cross product Fracture line length projection Vector (x)	Cross product Fracture line length projection Vector (y)	Cross product Fracture line length projection Vector (z)
1	290	0.6858	0.5334	150	82	0.50	-0.86	0.14	0.65	0.818639282	0.05	0.13	0.64
1	290	3.4033968	0.5334	140	75	0.62	-0.74	0.26	0.55	0.973460633	0.09	0.24	0.48
1	290	5.5626	0.5334	205	68	-0.39	-0.84	0.37	1.00	0.53515017	0.13	0.35	0.92
1	290	7.8486	0.5334	140	81	0.63	-0.76	0.16	0.52	1.029672541	0.05	0.15	0.49
									Frac Density Line 1	0.7647325 8			

Table 35 Sample 5

Scan Line	Trend	Fracture Distance (M)	Fracture Length (M)	Fracture Strike	Fracture Dip	Fracture Vector x coord	Fracture Vector y coord	Fracture Vector z coord	Weighting factor for line length	Weighted Fracture Length	Cross product Fracture line length projection Vector (x)	Cross product Fracture line length projection Vector (y)	Cross product Fracture line length projection Vector (z)
1	280	0.2795016	0.100584	125	83	0.81	-0.57	0.12	0.44	0.230267841	0.02	0.12	0.42
1	280	0.9906	0.1271016	145	90	0.57	-0.82	0.00	0.71	0.179748807	0.00	0.00	0.71
1	280	3.4542984	0.1271016	150	85	0.50	-0.86	0.09	0.77	0.16547743	0.02	0.09	0.76
1	280	6.3246	0.1271016	150	84	0.50	-0.86	0.10	0.77	0.165284805	0.02	0.10	0.76
									Frac Density Line 1	0.844259323			

Table 36 Sample 6

Scan Line	Trend	Fracture Distance (M)	Fracture Length (M)	Fracture Strike	Fracture Dip	Fracture Vector x coord	Fracture Vector y coord	Fracture Vector z coord	Weighting factor for line length	Weighted Fracture Length	Cross product Fracture line length projection Vector (x)	Cross product Fracture line length projection Vector (y)	Cross product Fracture line length projection Vector (z)
1	290	0.1524	1.2444984	165	80	0.25	-0.95	0.17	0.83	1.508144666	0.06	0.16	0.81
1	290	2.489301 6	1.2954	190	90	-0.17	-0.98	0.00	0.98	1.315383633	0.00	0.00	0.98
1	290	4.978298 4	1.2954	170	90	0.17	-0.98	0.00	0.87	1.495799077	0.00	0.00	0.87
1	290	8.204301 6	1.2954	180	90	0.00	-1.00	0.00	0.94	1.378535886	0.00	0.00	0.94
									Frac Density Line 1	0.5344774 7			

Table 37 Sample 7

Scan Line	Trend	Fracture Distance (M)	Fracture Length (M)	Fracture Strike	Fracture Dip	Fracture Vector x coord	Fracture Vector y coord	Fracture Vector z coord	Weighting factor for line length	Weighted Fracture Length	Cross product Fracture line length projection Vector (x)	Cross product Fracture line length projection Vector (y)	Cross product Fracture line length projection Vector (z)
1	280	0.1524	0.4572	195	87	-0.26	-0.96	0.05	1.00	0.458941619	0.01	0.05	0.99
1	280	0.4572	0.6858	210	85	-0.50	-0.86	0.09	0.94	0.729446191	0.02	0.09	0.94
1	280	1.2445898 4	0.6858	205	84	-0.42	-0.90	0.10	0.97	0.709714086	0.02	0.10	0.96
1	280	1.4730984	0.6858	210	86	-0.50	-0.86	0.07	0.94	0.729578006	0.01	0.07	0.94
1	280	2.5655016	0.6858	200	85	-0.34	-0.94	0.09	0.98	0.696297352	0.02	0.09	0.98
1	280	4.572	0.6858	200	90	-0.34	-0.94	0.00	0.98	0.69637957	0.00	0.00	0.98
1	280	5.6897016	0.6858	165	90	0.26	-0.97	0.00	0.91	0.756696577	0.00	0.00	0.91
									Frac Density Line 1	1.202801751			

APPENDIX D

FINAL CORRELATION CALCULATIONS

Table 38

Outcrop	Fracture Density M^{-1}	Poisson Ratio dry	Vp dry (ft/sec)	Vs dry (ft/sec)	$(Vp/Vs)^2$	Density dry (gm/cc)	porosity (%)	Rock type
Locality 1	0.304	0.314	17141.733	8917.126	3.695	2.585	3.800	Lower K Limestone - Fossiliferous - Fine grained Limestone
Locality 2	3.600	0.269	14620.670	8224.147	3.160	2.490	6.900	Limestone
Locality 3	1.374	0.345	14810.696	7209.646	4.220	2.516	5.520	Limey Shales
Locality 4	0.765	0.374	21422.245	9618.111	4.961	2.671	2.827	Carbonate Siltstone
Locality 5	0.844	0.313	15630.906	8155.184	3.674	2.267	7.015	Limestone
Locality 6	0.534	0.375	24354.660	10904.856	4.988	2.283	7.700	Carbonate Siltstone
Locality 7	1.203	0.342	14458.006	7078.412	4.172	2.456	0.600	Shale

Table 39

Conversion to SI Units	Fracture Density M^{-1}	Young's Modulus dry (Pa)	Shear Modulus dry (Pa)	v/(1-2v)	Poisson Ratio dry	Vp dry (M/sec)	Vs dry (M/sec)	$(Vp/Vs)^2$	Density dry (kg/M^3)	Fracture Toughness KIC*10^6 = 0.313+0.027E *10^9	Ua = $(KIC)^2/(4mu(1+v))$	porosity (%)	Rock type
Locality 1	0.304	2.90E+10	1.91E+10	0.848	0.314	5224.800	2717.940	3.695	2584.500	1097314.466	1.20E+01	3.800	Lower K Limestone - Fossiliferous - Fine grained Limestone
Locality 2	3.600	2.47E+10	1.56E+10	0.580	0.269	4456.380	2506.720	3.160	2489.714	978948.436	1.21E+01	6.900	Limestone
Locality 3	1.374	1.81E+10	1.21E+10	1.110	0.345	4514.300	2197.500	4.220	2515.667	800832.825	9.81E+00	5.520	Limey Shales
Locality 4	0.765	3.34E+10	2.30E+10	1.480	0.374	6529.500	2931.600	4.961	2670.909	1215299.450	1.17E+01	2.827	Carbonate Siltstone
Locality 5	0.53447747	3.67E+10	2.52E+10	1.49398744	0.374623082	7423.300238	3323.800106	4.987974877	2283.444444	1303992.511	1.23E+01	7.7	Carbonate Siltstone

Locality 6	0.844259323	2.13E+10	1.40E+10	0.83683768	0.313991507	4764.300152	2485.70008	3.673675368	2267.384615	889175.1065	1.07E+01	7.015384615	Limestone
Locality 7	1.203	1.70E+10	1.14E+10	1.086	0.342	4406.800	2157.500	4.172	2455.889	772866.224	9.73E+00	0.600	Shale

Table 40

	v/(1-2v)	**(Fd*Ua/Gs)*10^{9}**
Locality 1	0.848	1.913E-01
Locality 2	0.580	2.778E+00
Locality 3	1.110	1.110E+00
Locality 4	1.480	3.901E-01
Locality 5	0.836837684	0.409955569
Locality 6	1.493987438	2.597E-01
Locality 7	1.086	1.024E+00

Table 41

E11*10^4	Sample 6	Sample 4	Sample 2	Sample 1	Sample 3	Sample 7
0.1	0.354904261	0.337239574	0.179167212	0.238322326	0.154811051	0.153834514
0.2	1.419617045	1.348958295	0.716668849	0.953289305	0.619244203	0.615338055
0.3	3.194138352	3.035156164	1.612504911	2.144900935	1.393299456	1.384510625
0.4	5.678468181	5.395833181	2.866675397	3.813157219	2.476976811	2.461352221
0.5	8.872606533	8.430989346	4.479180307	5.958058154	3.870276268	3.845862846
0.6	12.77655341	12.14062466	6.450019642	8.579603742	5.573197826	5.538042498
0.7	17.3903088	16.52473912	8.779193402	11.67779398	7.585741485	7.537891178
0.8	22.71387272	21.58333272	11.46670159	15.25262887	9.907907246	9.845408886
0.9	28.74724517	27.31640548	14.5125442	19.30410842	12.53969511	12.460595621
1	35.49042613	33.72395738	17.91672123	23.83223262	15.48110507	15.383451384
1.1	42.94341562	40.80598843	21.67923269	28.83700147	18.73213714	18.613976174
1.2	51.10621363	48.56249863	25.80007857	34.31841497	22.2927913	22.152169993

REFERENCES

1. Wickham, J.S. & Yu, X.B. 2012. Geomechanics and Fracture Density: Understanding the Theory.
2. Backers, T. 2005. Fracture toughness determination and micromechanics of rock under mode **I** and mode II loading. PhD thesis, University of Potsdam

3. Barthelemy, J-F, MLE Guiton and J-M Daniel. 2009. Estimates of Fracture Density and Uncertainties from Well Data. International Journal of Rock Mechanics and Mining Sciences 46, (3): 590-603

4. Barton, C.C. 1995. Fractal Analysis of Scaling and Spatial Clustering of Fractures. In C.C. Barton and P.R. LaPointe, eds., Fractals in the Earth Sciences: New York, Plenum Press: 141-178.

5. Bourne, S.J., and E.J. Willemse. 2001. Elastic Stress Control on the Pattern of Tensile Fracturing around a Small Fault Network at Nash Point, United Kingdom. Journal of Structural Geology 23: 1753-1770

6. Busetti, S., K. Mish, Z. Reches, 2012. Damage and plastic deformation of reservoir rocks: Part 1. Damage Fracturing. AAPG Bulletin 96 (9): 1687-1709.

7. Busetti, S., K. Mish, P. Hennings, Z. Reches, 2012. Damage and plastic deformation of reservoir rocks: Part 2. Propagation of a hydraulic fracture. AAPG Bulletin 96 (9): 1711-1732.

8. Chiles, J.P., H. Beucher, H. Wackernagel, C. Lantuejoul, P. Elion. 2008. Estimating fracture density from a linear or aerial survey. Proceedings of the VIII International Geostatistics Congress, *ed.* J. Ortiz and X. Emery. V. 1, p. 535-544. http://downloads.gecamin.cl/cierreeventos/geostats2008/prsntcns/00158 00721 p r.pdf.

9. Corbett, K., M. Friedman and J. Spang. 1987. Fracture Development and Mechanical Stratigraphy of Austin Chalk, Texas. AAPG Bulletin 71 (1): 17-28

10. Dershowitz, W.S. and H.H. Herda. 1992. Interpretation of Fracture Spacing and Intensity. In J.R. Tillerson and W.R. Wawersik, eds., Proceedings of the 33rd U.S. Symposium on Rock Mechanics. Rotterdam, Balkema: 19-30

11. Di Naccio, D., P. Boncio, S. Cirilli, F. Casaglia, E. Morettini, G. Lavecchia and F. Brozzetti. 2005. Role of Mechanical Stratigraphy on Fracture Development in Carbonate Reservoirs; Insights from Outcropping Shallow Water carbonates in the Umbria-Marche Apennines, Italy. Journal of Volcanology and Geothermal Research 148, (1-2): 98-115.

12. Ehlen J. 2000. Fractal Analysis of Joint Patterns in Granite. International Journal of Rock Mechanics and Mining Sciences 37: 909-922.

13. Gdoutos E.E. 2005. Fracture Mechanics, An Introduction.

14. Gillespie, P.A., G.B. Howard, J.J. Walsh, and J. Watterson. 1993. Measurement and Characterization of Spatial Distributions of Fractures. Tectonophysics 226: 113-141

15. Griffith, A. A. 1921. The Phenomena of rupture and flow in solids. Philosophical Transactions of the Royal Society A221: 163-198.

16. Hennings, P.H., J.E. Olson and L.B. Thompson. 2000. Combining Outfrop Data and three-dimensional Models to Characterize Fractured Reservoirs: An Example from Wyoming. AAPG Bulletin 84, (6): 830-849

17. Huang, Q., and J. Angelier. 1989. Fracture Spacing and its Relation to Bed Thinkness. Geological Magazine 126: 355-362

18. Irwin, G. R., 1956. Onset of Fast Crack Propagation in High Strength Steel and Aluminum Alloys, Sagamore Research Conference Proceedings, Vol. 2, 289-305.

19. Julander, D.R., P.F. Cowell, H. Wu, and J.A. Angehrn. 1999. An Investigation of Subsurface Fracture Distribution in the Monterey Formation, Lost Hills Oil Field, CA using Borehole Image Logs and Whole Core. AAPG Bulletin 83, (4): 692-692

20. Karaman, A., and P.J. Carpenter. 1997. Fracture Density Estimates in Glaciogenic Deposits from P-wave Velocity Reductions. Geophysics 62, (1): 138-148.

21. Ladeira, F.L. and N.J. Price. 1981. Relationship between Fracture Spacing and Bed Thickness. Journal of Structural Geology 3: 179-183

22. LaPointe, P.R. 1988. A Method to Characterize Fracture Density and Connectivity through Fractal Geometry. International Journal of Rock Mechanics and Mining Sciences & Geomechanics Abstracts 25 (6): 421-429

23. LaPointe, P.R. 2002. Derivation of Parent Fracture Population Statistics from Trace Length Measurements of Fractal Fracture Populations. lnternation Journal of Rock Mechanics and Mining Sciences 39: 381-388.

24. LaPointe, P.R. and J.A. Hudson. 1985. Characterization and Interpretation of Rock Mass Joint Pattern. Geological Society of America Special Paper 199: 1-37.

25. Lezin, C., F. Odonne, G.J. Massonnat and G. Escadeillas. 2009. Dependence of Joint Spacing on Rock Properties in Carbonate Strata. AAPG Bulletin 93 (2): 271-290

26. Lock, E.B., Peschier, L., Fife, A. and Wawak, B. 2010. Eagle Ford (Boquillas) Formation and Associated Strata in Val Verde County, Texas. South Texas Geological Society Guidebook 2012-01.

27. Lou, M., and J.A. Rial. 1997. Characterization of Geothermal Reservoir Crack Patterns using Shear-Wave Splitting. Geophysics 62 (2): 487-494

28. Mauldon, M., W.M. Dunne and M.B. Rohrbaugh. 2001. Circular Scanlines and Circular Windows; New Tools for Characterizing the Geometry of Fracture Traces. Journal of Structural Geology 23, (2-3): 247-258

29. Maultzsch, S., M. Chapman, E. Liu, X-Y. Li. 2003. Modeling Frequency Dependent Seismic Anisotropy in Fluid Saturated Rocks with aligned Fractures; Implication of Fracture Size Estimation from anisotropic Measurements. Geophysical Prospecting 51 (5): 381-392

30. Maxwell, S.C. and T.I. Urbancic. 2005. The Potential Role of Passive Seismic Monitoring for Real-Time 40 Reservoir Characterization. SPE Reservoir Evaluation and Engineering 8 (1): 70-76.

31. Mclennan, J.A., P.F. Allwardt, P.H. Hennings, and H.E. Farrell. 2009. Multivariate Fracture Intensity Prediction; Application to Oil Mountain Anticline, Wyoming. AAPG Bulletin 93, (11): 1585-1595.

32. McQuillan, H. 1974. Fracture Patterns on Kuh-e Asmari Anticline, Southwest Iran. AAPG Bulletin 58 (2): 236-246

33. Murray, G.H. 1968. Quantitative Fracture Study: Sanish Pool, McKenzie County, North Dakota. AAPG Bulletin 52, (1): 57-65.

34. Narr, W. and I. Lerche. 1984. A Method for Estimating Subsurface Fracture Density in Core. AAPG Bulletin 68, (5): 637-648

35. Narr, W. and J. Suppe. 1991. Joint Spacing in Sedimentary Rocks. Journal of Structural Geology 13: 1037-1048.

36. Ortega, O.J., R.A. Marratt and S.E. Laubach. 2006. A Scale-Independent Approach to Fracture Intensity and Average Spacing Measurement. AAPG Bulletin 90, (2): 193- 208

37. Page, Lincoln R. and Adams, John Emery. 1940. Stratigraphy, Eastern Midland Basin, Texas. AAPG Bulletin 24, (1): 52-208

38. Palchik, V. and Y.H. Hatzor. 2002. Crack Damage Stress as a Composite Function or Porosity and Elastic Matrix Stiffness in Dolomites and Limestones. Engineering Geology 63: 233-245

39. Peacock, D.C.E., S.D. Harris, and M. Mauldon. 2003. Use of Curved Scanlines and Boreholes to Predict Fracture Frequency. Journal of Structural Geology 25: 109-119.

40. Pollard, D.O., and P. Segal. 1987. Theoretical Displacements and Stresses near Fractures in Rock: With Applications to Faults, Joints, Veins, Dikes and Solution Surfaces, in B.K. Atkinson, ed., Fracture Mechanics of Rock: New York, Academic Press Geology Series: 277-349.

41. Priest, S.D. and J.A. Hudson. 1976. Discontinuity Spacings in Rock. International Journal of Rock Mechanics and Mining Sciences and Geomechanical Abstracts 13: 135-148.

42. Renshaw, C.E. 1997. Mechanical Controls on the Spatial Density of Opening-Mode Fracture Networks. Geology 25: 923-926

43. Schultz-Eia, D.O. and J. Yeh. 1992. Predicting Fracture Permeability from Bed Curvature. Proceedings of the 33rd U.S. Symposium on Rock Mechanics 33: 579-589

44. Sheriff, R.E., 1991, Encyclopedic Dictionary of Exploration Geophysics, 3rd ed. Society of Exploration Geophysics, Tulsa, OK

45. Shi, G. C. 1985. Mechanics and Physics of Energy Density Theory. Theoretical and Applied Fracture Mechanics 4: 157-173

46. Stearns, D.W. 1967. Certain Aspects of Fracture in naturally Deformed Rocks. In R.E. Riecker, ed. Rock Mechanics Seminar: US Air Force Cambridge Research Laboratories. Contribution AD 669375: 97-118.

47. Stearns, D.W. and M. Friedman. 1972. Reservoirs in Fractured Rock, in R.E. King, ed., Stratigraphic Oil and Gas Fields: Classification, Exploration Methods, and Case Histories. AAPG Memior 16: 82-106.

48. Tapp, B., S. McGinty-Davis, L. Lortz and M. Schlagel. 1999. Fracture Architecture of the Tensleep Sandstone, Bighorn Basin, Wyoming; Surface Analogs for Subsurface Reservoirs. AAPG Bulletin 83, (7): 1189-1189.

49. Veatch, R.W. 1983. Overview of Current Hydraulic Fracturing Design and Treatment Technology- Part I. Journal of Petroleum Technology 35, (4): 677-687

50. Velde, B.J., J. DuBois, G. Touchard, and A. Badri. 1990. Fractal Analysis of Fractures in Rocks: The Cantor's Dust Method. Tectonophysics 179: 345-352

51. Watts, N.L., 1983, Microfractures in Chalks of Albuskjell Field, Norwegian Sector, North Sea; Possible Origin and Distribution. AAPG Bulletin 67, (2): 201-234

52. Wickham, J. S., G. Tapp and J. Reddy, 1982, Finite-Element Modelling of Fracture Density in Single Layer Folds. International Journal for Numerical & Analytical Methods in Geomechanics 6: 441-459

53. Willemse, E.J.M., D.C.P. Peacock, A. Aydin and D.O. Pollard. 1997. Relationship between Faults and Fractures in Tight Reservoirs. AAPG Bulletin 81: 1419-1420.

54. Wright, Wayne R., 2011. Pennsylvanian Paleodepositional Evolution of the Greater Permian Basin, Texas and New Mexico: Depositional Systems and Hydrocarbon Reservoir Analysis. AAPG Bulletin 95 (9): 1525-1555

55. Wu, H. and D.D. Pollard. 1995. An Experimental Study of the Relationship between Joint Spacing and Layer Thickness. Journal of Structural Geology 17: 887-905

56. Wu, H. and D.O. Pollard. 2002. Imaging Fracture Networks around Boreholes. AAPG Bulletin 86 (4): 593-604.

57. Xu, X., and I. Tsvankin. 2007. A Case Study of Azmuthal AVO Analysis with Anisotropic Spreading Correction. Leading Edge 26, (12): 1552-1561.

58. Zahm, C. and P.H. Hennings. 2009. Complex Fracture Development Related to Stratigraphic Archetecture; Challenges for Structural Deformation Prediction, Tensleep Sandstone at the Alcove Anticline, Wyoming. AAPG Bulletin 93, (11): 1427-1446

BIOGRAPHICAL INFORMATION

Sean Kimiagar is a Petroleum Geologist. He earned his Bachelor of Science degree in Petroleum Geosciences Engineering from Petroleum Institute in Abu Dhabi and Master of Science degree in Petroleum Geology from University of Texas at Arlington. Sean's research interests include structural geology, petroleum systems and petroleum industry economics. In his professional career, he has had two industry internships as a geologist, one with Abu Dhabi National Oil Company, and the other with BHP Billiton Petroleum. Sean is currently a Geologist and Earth Modeler at Halliburton, in Houston, Texas and plans to grow and develop as a respected geologist and professional in the energy industry.